T.R.
BOLU ABANT İZZET BAYSAL UNIVERSITY
INSTITUTE OF GRADUATE STUDIES
Department of Physics

ENHANCEMENT OF SUPERCONDUCTING PROPERTIES OF NANO-SIZE YITTRIUM BASED SUPERCONDUCTORS

DOCTOR OF PHİLOSOPHY

GÜLNUR KURTUL

ACADEMIC SUPERVISOR
Prof. Dr. CABİR TERZİOĞLU

BOLU, OCAK - 2023

APPROVAL OF THE THESIS

Enhancement of superconducting properties of nano-size yittrium based superconductors submitted by **Gülnur KURTUL** and defended before the Examining Committe Members listed below in partial fulfillment of the requirements for the degree of **Doctor of Philosophy** in **Department of Physics, Institute of Graduate Studies of Bolu Abant Izzet Baysal University in 30.01.2023** by

Examining Committee Members	**Signature**
Supervisor Prof. Dr. Cabir TERZİOĞLU University of Bolu Abant İzzet Baysal	....
Member Prof. Dr. Osman GÖRÜR University of Bolu Abant İzzet Baysal	....
Member Prof. Dr. Gürcan YILDIRIM University of Bolu Abant İzzet Baysal	....
Member Associate Prof. Dr. Yusuf ZALAOĞLU University of Osmaniye Korkut Ata	....
Member Associate Prof. Dr. Mustafa Burak TÜRKÖZ University of Karabük	....

Prof. Dr. İbrahim KÜRTÜL

Director of Instıtute of Graduate Studies

ETHICAL DECLARATION

In this thesis dissertation that was properly prepared according to the Thesis Writing Rules of Bolu Abant İzzet Baysal University of the Institute of Graduates Studies, I hereby declare that;

- All data, information, and documents presented in the thesis were obtained in accordance with the academic and ethical rules,
- All data, documents, assessments, and results were presented in accordance with the scientific ethical and moral rules,
- All works that were benefitted in the thesis were appropriately cited,
- No alteration was made in the data used,
- Study presented in this thesis is original,

Otherwise, I declare that I accept the loss of all my rights in case any contradiction that may arise against me.

Based on the plagiarism report that was generated on the date of 30/01/2023 by using predetermined filtrations set by Directorate of Institute of Graduate Studies of the Turnitin programme, a plagiarism detections of ware, the similarity index detectedwas 19 %.

GÜLNUR KURTUL

ABSTRACT

ENHANCEMENT OF SUPERCONDUCTING PROPERTIES OF NANO-SIZE YITTRIUM BASED SUPERCONDUCTORS

PHD THESIS
GÜLNUR KURTUL
BOLU ABANT IZZET BAYSAL UNIVERSITY
INSTITUTE OF GRADUATE STUDIES
DEPARTMENT OF PHYSICS
(SUPERVISOR:PROF.DR. CABİR TERZİOĞLU)

BOLU, JANUARY 2023
(xii + 66)

In this work, the role of oxygen and Mn_2O_3 impurity roles on the basic characteristic features of $YBa_2Cu_3O_{7-y}$ superconductors was investigated. While preparing the samples, it was prepared by solid state reaction method by adding Mn with varying additive ratio instead of copper. The samples were annealed for 24 hours at 945 °C and at room temperature such that the temperature increased by 3 °C /min at 945 °C and decreased by 1 °C /min. The characteristics of the samples were made by taking X-ray diffraction patterns, scanning electron microscopy (SEM), DC electrical Resistivity Tests measurements. As a result of XRD and SEM measurements, when oxygenated samples are compared with oxygen-free sample, the presence of oxygen improves the appearance of surface morphology and crystallinity quality for YBa2Cu3O7-y superconductors. At the same time, it was found that the increase in manganese impurity of Mn-doped YBa2Cu3O7-y superconductors prepared under oxygen annealing ambient conditions significantly changed grain alignment distributions and orientations, grain boundary regions, interaction quality between grains and basic structural morphology appearances. itis also seen that the transition temperature and critical current density increase when Mn doping is compared with Mn undoping and also the oxygen ambient condition has ben noted to affect positively the values of Jc parameter. According to these results, it was seen that Oxygen and Mn doped had a positive effect on YBCO.

KEYWORDS: XRD, Sem, YBCO, Superconductor, Mn

ÖZET

NANO-BOYUTTA YITTRIUM TEMELLI ÜSTÜNILETKENLERIN SÜPERILETKENLIK ÖZELLIKLERININ IYILEŞTIRILMESI

DOKTORA TEZİ
GÜLNUR KURTUL
BOLU ABANT İZZET BAYSAL ÜNİVERSİTESİ
LİSANSÜSTÜ EĞİTİM ENSTİTÜSÜ
FİZİKANABİLİM DALI
KATIHAL FİZİK BİLİM DALI
(TEZ DANIŞMANI:PROF.DR.CABİR TERZİOĞLU)

BOLU, OCAK - 2023
(xii+ 66)

Bu çalışmada, oksijen ve Mn_2O_3 safsızlığının YBCO süperiletkenlerinin temel karakteristik özellikleri üzerindeki rolü incelenmiştir. Numuneler hazırlanırken bakır yerine değişen katkı oranlarında Mn ilave edilerek katı hal reaksiyonu yöntemiyle hazırlanmıştır. Numuneler 24 saat 945 °C'de ve oda sıcaklığında 945 °C'de sıcaklık 3 C^o/dk artacak ve 1 C^o/dk azalacak şekilde tavlanmıştır. Numunelerin özellikleri X-ışını kırınım, taramalı elektron mikroskobu (SEM), DC elektriksel direnç ölçünler alınarak yapılmıştır. XRD ve SEM ölçümleri sonucunda, oksijenli numuneler ile oksijensiz numuneler karşılaştırıldığında, oksijenin varlığı YBa2Cu3O7-y süper iletkenler için yüzey morfolojisinin görünümünü ve kristallik kalitesini iyileştirmektedir. Aynı zamanda, oksijen tavlama ortam koşullarında hazırlanan Mn katkılı YBa2Cu3O7-y süperiletkenlerin manganez safsızlığındaki artışın, tane dizilim dağılımlarını ve yönelimlerini, tane sınır bölgelerini, taneler arasındaki etkileşim kalitesini ve temel yapısal morfoloji görünümlerini önemli ölçüde değiştirdiği bulunmuştur. Ayrıca Mn katkılama ile Mn katkısızlaştırma karşılaştırıldığında geçiş sıcaklığının ve kritik akım yoğunluğunun arttığı görülmektedir. Ayrıca oksijen ortam koşulunun da J_c parametresi değerlerini olumlu etkilediği kaydedilmiştir. Bu sonuçlara göre Oxygen ve Mn katkılının YBCO üzerinde olumlu etkisi olduğu görülmüştür.

ANAHTAR KELİMELER: XRD, Sem, YBCO, Süperiletkenlik, Mn

TABLE OF CONTENTS

PAGE

APPROVAL OF THE THESIS...ii

ETHICAL DECLARATION..iii

ABSTRACT...iv

ÖZET.................. v

TABLE OF CONTENTS vi

LIST OF FIGURES...vii

LIST OF TABLES..viii

LIST OF PICTURES x

LIST OF ABBREVIATIONS AND SYMBOLS..xi

1. INTRODUCTION.. 1

2. AIM AND SCOPE OF THE STUDY 2

2.1 Overview of Superconductors..5

2.1.1 Structure of YBCO System 8

3. MATERIALS AND METHODS 11

3.1 $YBa_2Cu_3O_{7-y}$ Superconductor Preparation Procedure.....................11

3.2 Experimental Methods for Measurements..14

3.2.1 Electrical Resistivity Tests 14

3.2.2 X-Ray Diffraction Measurements 15

3.2.3 SEM Experimental Measurements 16

3.2.4 Transport Critical Current Density Measurements.............................. 17

4. RESULTS AND DISCUSSION 18

4.1 Change of General Resistivities Grounded on Dc Electrical Experiments...18

4.1.1 Evolution of Superconducting Quantities of Bulk $YBa_2Cu_3O_{7-y}$ Superconductors with Manganese Impurity and Oxygen Ambient……....26

4.1.2 Alteration of Charge Carrier Concentrations in Valence Bands of Perovskite-Based $YBa_2Cu_3O_{7-y}$ Cuprate Superconductors with Manganese Impurity and Oxygen Ambient... 29

4.2 Changes in Transport Critical Current Density Searches................33

4.3 SEM Analysis..37

4.4 XRD Diffractogramsfor $YBa_2Cu_3O_{7-y}Mn_x$ Ceramic Compounds Prepared at Different Annealing Ambient Conditions...............................45

4.5 EDX Results of Bulk $YBa_2Cu_3O_{7-y}Mn_x$ Systems Prepared................55

5. REFERENCES.. 58

LIST OF FIGURES

Page

Figure 4.1: Pure and Mn added bulk $YBa_2Cu_3O_{7-y}$ superconductors prepared at without the oxygen ambient condition. 31
Figure 4.2: Pure and Mn added $YBa_2Cu_3O_{7-y}$superconductors produced under the oxygen ambient condition. 31
Figure 4.3: Two pure samples prepared at oxygen and oxygen-free annealing ambient. 32
Figure 4.4: The pure superconductors produced with oxygen annealing ambient condition. 39
Figure 4.5: The pure superconductors produced without oxygen annealing ambient condition. 39
Figure 4.6: Sem photographics of Mn(0.01) added YBCO superconductors prepared at the Oxygeb ambient conditions. 40
Figure 4.7: Sem photographics of Mn(0.03) added YBCO superconductors prepared at the Oxygen ambient conditions. 41
Figure 4.8: Sem photographics of Mn(0.05) added YBCO superconductors prepared at the Oxygen ambient conditions. 42
Figure 4.9: Sem photographics of Mn(0.07) added YBCO superconductors prepared at the Oxygeb ambient conditions. 43
Figure 4.10: Sem photographics of Mn(0.10) added YBCO superconductors prepared at the Oxygen ambient conditions. 43
Figure 4.11:Sem photographics of Mn(0.30) added YBCO superconductors prepared at the Oxygeb ambient conditions. 44
Figure 4.12: Pure and Mn added bulk $YBa_2Cu_3O_{7-y}$superconductors prepared at without the oxygen ambient condition. 53
Figure 4.13: Pure and Mn added $YBa_2Cu_3O_{7-y}$superconductors produced under the oxygen ambient condition. 53
Figure 4.14: YBCO under oxygen and without oxygen 54

LIST OF TABLES

Page

Table 4. 1: Electrical resistivity parameters oxygen Free ambient. 24
Table 4. 2: Electrical Resistivity Parameters with Oxygen Ambient.............. 25
Table 4. 3: Experimental data Oxygen free ambient. 35
Table 4. 4: Experimental data with oxygen ambient....................................... 36
Table 4. 5: Distribution of chemical components throughout the bulk $YBa_2Cu_3O_{7-y}Mn_x$ superconductors produced under the oxygen ambient. 57

LIST OF PICTURES

Page

Picture 3.1: YBCO from Alfa Aesar exclusive distributor, the high purity of about 99.99%......13
Picture 3. 2: Measuring devices used in sample preparation. 13
Picture 3. 3: Experimental set up for the 4-point probe measurement. 15
Picture 3. 4: Cyclic cryogenic refrigeration system......15
Picture 3. 5: X-ray diffractometer system......16

LIST OF ABBREVIATIONS AND SYMBOLS

Mn	: Manganeze
SEM	: Scanning electron microscope
XRD	: X-ray diffraction
YBCO	: $YBa_2Cu_3O_{7-y}$(Y_{123})
a,b,c	: Lattice parameters
ρ	: Resistivity
T_C	: Critical Temperature
P_{hole}	: Hole concentrations
ρ_{res}	: Residual resistivity
bcc	: Basic cubic center
J_c:	: Critical current density
FWHM	: Full Width at Half Maximum

ACKNOWLEDGEMENTS

This thesis would not have been possible without the help of my supervisors Prof. Dr. Cabir TERZİOĞLU and Prof.Dr. Gürcan YILDIRIM. This field of superconductivity was fairly new to me. I would not have been able to digest the vast amount of without the help of the them. Not only has they helped me understand difficult concepts and experimental procedures, they have also been a constant support during times of distress.

I am also indebted to my husband İbrahim KURTUL, who have helped me in every step of the way.

My special thanks to Elif ERBAŞ for their unlimited moral support when I felt the need for it.

Lastly, I would also want to express my sincere thanks to my family members and friends, who have given me the much needed moral support.

For memory of my dear mother-in-law Ayşe SÖĞÜTOĞLU KURTUL died in 04.01.2022…

1. INTRODUCTION

Throughout history, technology and industry have extensively been developed to serve the requirements of human beings for daily life as much as possible. Thus, with rapid advances in technology, the desire of human beings to keep pace with technology, and the increase in the world population growth day by day, energy consumption has considerably been increasing, and therefore many more natural resources have been being demolished. In this context, excess energy use should be avoided or limited as much as possible in all application areas. To illustrate, energy distribution constitutes the basis of energy consumption problems in industrial power systems and energy related sectors. Thus, energy efficient systems in the application areas have been sought to leave a cleaner world for future generations. That is exactly why superconductors (Type-I or Type-II ceramic samples) exhibiting no resistance (energy lossless) and higher current and magnetic field carrying capacities have been come across in the potential application fields for several years. In other words, the preference for type-I or Type-II superconductors have provided a valuable incentive for the efficient use of energy, and the activities in daily life have been performed without any compromise but in low energy consuming. Correspondingly, superconductors have provided reliable, clean, economical, cheap, energy-efficient, and power quality to humanity. Shortly, the preference for superconductors or their replacement with traditional metallic materials in industrial power systems and energy-related sectors seems to be one of the only solutions to overcome emerging energy-saving and ecological energy problems and to secure the world for future generations for the environmentally conscious climate protection, resource conservation, and cost savings. At the same time, the Type-I or Type-II superconductors play a crucial role in monitoring energy production, protection, conservation, consumption, distribution, storage, supply-demand balance, energy management planning, and operation.

2. AIM AND SCOPE OF THE STUDY

In the current work, we have determined the oxygen and Mn_2O_3 impurity roles on the basic characteristic features of $YBa_2Cu_3O_{7-y}$ superconductors. On this basis, we have initially produced the pure $YBa_2Cu_3O_{7-y}$ superconductor under ambient annealing conditions with and without oxygen to answer the question appears that which annealing medium provides the material produced show higher basic characteristic features enabling the material to use in much more application fields. The experimental results obtained have shown that the presence of oxygen has increased the stabilization of orthorhombic phase in the pure $YBa_2Cu_3O_{7-y}$ superconducting system. Afterward, the effect of different Mn_2O_3 impurity addition amounts ($0.00 \leq x \leq 0.30$) on the basic characteristic features of $YBa_2Cu_3O_{7-y}$ superconductors produced under oxygen and oxygen-free has extensively been examined by means of electrical conductivity, X-ray diffraction, critical current density, scanning electron microscopy, and related theoretical results. Moreover, we can explain why the addition of Mn atoms in the $YBa_2Cu_3O_{7-y}$ superconducting system are preferred in the comprehensive work. The manganese (Mn) in the transition metal parents exhibits the paramagnetic property with the molar magnetic susceptibility value and crystallizes in the body centered cubic (bcc) crystallographic structure.

It should be mentioned that the presence of the manganese in the system leads to the increment in the magnetic interactions between both all the paramagnetic (foreign and host) ions and these paramagnetic ions and the crystal field. Correspondingly, the coexistence of superconductivity and magnetism is a problem worth investigating. Moreover, the Mn and related alloys are used to develop the workability, mechanical strength, and resistivity to wear due to the mechanical hardness, easy oxidization (oxidizing agent), and stabilization [1]. Besides, the Mn-containing materials have widely been used in the production of ceramics, glasses, and fertilizers. In the metallurgical application fields the manganese material possesses satisfactory substitute for the zinc and vanadium materials. Moreover, the Mn with the superior deoxidizing, and alloying features is one of the most preferred materials to improve the malleability of iron and steel. Correspondingly, the manganese is the most important component for the low-cost stainless steel with hightensile strength (≈863 MPa) [2-5]. In this respect, the steel production process supplies most of the manganese demand currently in the range from 85% to 90% of total demand [6,7]. Besides, the presence of manganese has been known to develop the workability of steel at relatively higher temperature values. Hence, the manganese addition level of roughly 1.5% in the Al-based alloys has enhanced the resistivity towards the corrosion [8]. At the same time, the manganese has been used in the different application fields such as the neutralization of the greenish tinge in glass [9], drying black paints, manufacture of oxygen and chlorine, activator in potential red-emitting phosphors, and the gasoline for the performance improvement [10]. It is also possible to see in application areas including the biological warfare against harmful bacteria, biochemistry, dry cell battery, ceramic coloring, minting technology, shunt resistors and newer alkaline battery technologies [11-18].

It is observed from the application fields of manganese material that the Mn atoms can easily integrate to the host crystal structures by new chemical or ionic bonds. Therefore, it is obvious that the Mn atoms support the formation of other crystal structures; namely, the tetragonal, triclinic, and orthorhombic crystal systems [19]. With the crystallographic structure the manganese seems to be one of the ideal materials to both diffuse rapidly throughout the granular structures such as the high temperature superconductors and integrate to the host atoms easily depending on the driving forces of annealing temperature and annealing time. Additionally, the manganese exhibits various chemical configurations as regards atomic occupancy ratios, density, ionic radius dimensions, cation-vacancy, bulk modulus, mechanical performances, electrical resistivity, electronegativity, electron affinity, valance electron states, thermal expansion, electron of the outer shell, thermal conductivity, electrical transmission, magnetic ordering, ionization energy, chemical potential, electrophilicity, valence electron states, magnetic moment magnitude and molar magnetic susceptibility properties from the main $YBa_2Cu_3O_{7-y}$ crystal matrix. Correspondingly, the addition of manganese in the $YBa_2Cu_3O_{7-y}$ system re-modifies the local atomic charges, ionization potential, surface nucleation growths, charge reservoir regions, chemical stability, oxygen content level, thermodynamic stability, charge transfer index, Cu-O coordination, stabilization of structure, formation of orbital hybrids, carrier concentrations, antiferromagnetic spin fluctuation, spin-density wave systems, percolative paths, bond distances of Cu-O planes, pair wave function, orbital hybridization mechanism, and copper oxidation states, activation energies, re-ordering of Cu-O bonds, atomic disorders, crystallization reaction kinetics, vibrational frequencies, and re-modification of skeleton geometrical structures (bond distances, angles, and dihedrals) of host matrix. Namely, with the valuable features mentioned above of manganese the basic characteristics (electrical, flux pinning ability, stabilization of system, bulk density, morphological, crystallinity quality, pairing mechanism, grain boundary couplings, structural, orbital hybridization mechanisms, and mechanical performance properties) of $YBa_2Cu_3O_{7-y}$ system are thought to improve considerably. Additionally, the manganese with the bcc crystallographic structure is anticipated to decrease dramatically the non-recoverable microscopic problems, and grain misorientations based on the improvement in the grain boundary couplings between the adjacent layers in thebulk$YBa_2Cu_3O_{7-y}$ crystal system. To sum up, the manganese is one the ideal compound to improve the basic characteristics of the $YBa_2Cu_3O_{7-y}$ superconductors. On this basis, in this comprehensive work, the influence of various Mn_2O_3 impurity addition amounts intervals of $0.00 \leq x \leq 0.30$ on the basic characteristic features of $YBa_2Cu_3O_{7-y}$ superconductors produced under oxygen and oxygen-free has been inspected by using the electrical conductivity, X-ray diffraction, critical current density, and related theoretical relations. It has been observed that the optimum manganese addition amount has improved the basic characteristic features of $YBa_2Cu_3O_{7-y}$ superconductors for usage in the potential application areas. Even, it has been found that the deficiency content level in the $YBa_2Cu_3O_{7-y}$ crystal structure has resulted in the departure from the orthorhombic distortion (orthorhombicity) or the oxygen ordering degree in the short-range ordered antiferromagnetic Cu-O chains.

2.1 Overview of Superconductors

The first superconductor (metallic mercury) was discovered in 1911 by observing no resistance under the applied current in the temperature-dependent electrical resistance test. Immediately after, the superconducting phenomenon was described by two important physical quantities: (I) exhibition of resistance after the critical transition temperature for a material, and (II) disappearance of magnetic flux fields before the critical transition temperature [20].

Over time, it has observed that many materials including the elements, semi-metals, semi-metal-containing compounds, metals, sulfides, carbides, alloys, rare earth borocarbides, organic materials, fullerenes, nitrides, heavy fermions, chevrel phase, A-15 inorganic samples, magnesium diboride, ruteno-cuprate samples, metal-based samples, carbon-containing compounds, chalcogens, silicon-based samples, iron-based materials, pyrochlorine oxides, and oxygen deficit perovskite-based cuprate Type-II materials have shown superconductivity until today [21, 22]. In the year of 1986, the first Type-II superconductor, $La_{2-x}Ba_xCuO_4$,was discovered with the transition temperature of nearly 35 K [23, 24]. After the breaking point for the superconductivity, yttrium has been replaced by lanthanum in the $La_{2-x}Ba_xCuO_4$ system, and hence $YBa_2Cu_3O_{7-y}$ compoundwas the first material discovered material exhibiting the transition temperature greater than the liquid nitrogen [25, 26]. On this basis, the superconductors are defined in two parents: soft Type-I materials and oxygen deficit perovskite-based cuprate Type-II samples [27–29]. Of the parents, the Type-II superconductors possessed relatively higher transition temperatures greater than the liquid nitrogen of 77 K, larger magnetic field and especially current carrying capability with lower energy consumption and losses at transition temperature ranges [30–32]. Thus, the discovery of perovskite-based cuprates with short-range ordered antiferromagnetic Cu-O chains and layers has opened the new potential application areas for the superconductors [33, 34]. Additionally, after the discovery, the latter parents have widely been preferred to use in the industrial power systems and energy-related sectors due to their intrinsic superior characteristic properties, viz. higher thermodynamic stability, optical and electronic characteristics, and resistance to the humidity environments, as well as the easy access to starting chemicals, simple chemical (light, abundant, low cost, and nonpoisonous) compositions, easy access to cooling refrigerant, easily deforming/shaping/rolling for long cables, wires (≈ higher than one kilometer length) and tape-casting constructions, easily accessible of nitrogen for cooling system, and stability to compositions and oxygen contents [35–38]. Similarly, not only the assistance in grid stabilization, and capacity expansion but also reduction in the CO_2 emissions and energy consumption are an important parameter in increasing the usage of materials in the potential application areas. Due to the alluring features mentioned above the oxygen deficit perovskite-based cuprate Type-II samples have widely found many application fields such as materials engineering, global electric power network, application-oriented material science, electro-optic, future cryo/refrigeration and hydrogen society, innovative and advanced energy infrastructure, heavy-industrial technology, sensitive process control, medical diagnosis (magnetic resonance imaging and treatments), fault current limiter, levitated trains, electric power transmission cable productions, magnetic separation, nuclear magnetic resonance, hydrogen society, innovative and advanced engineering, motors, generators, magnetic energy storage, renewable energy technologies, metallurgical, refrigeration, spintronics, heavy-industrial technologies, particle accelerators, industrial power systems and energy-related sectors [39–44] for several years.

On the other hand, some difficulties including the coexistence of multiple phase compositions, structural characteristic problems, low operating temperatures (can further be enhanced),sensitivity to applied current and magnetic field strengths, layered anisotropic structure, spatial characteristic of mobile carriers and electro-phonon couplings, misoriented microcrystals, large penetration depth, low charge carriers, mechanical stabilization, brittleness, grain boundary couplings between the adjacent layers, and short coherence length have needed to be improved to pave the way for and increase the usage of superconductors in the application fields [45–49]. However, it is well known that the limiting factors can be fixed as much as possible by means of the improvements in sample preparation methods such as calcination-sintering times/temperatures, dopant types, annealing ambient conditions, heat-treatment methodology, composition purity, and palletization loads/times/environments, as well as the operational procedures including the transition metal evaporation/diffusion on the surface, chemical addition, partial cationic/anionic substitution, chemical doping, metallic interfaced and metallic multilayered structures [50–55]. Particularly, the partial cationic/anionic substitution and chemical addition processes are relatively easy procedures to improve the basic characteristics (electrical, flux pinning ability, stabilization of system, bulk density, morphological, crystallinity quality, pairing mechanism, grain boundary couplings, structural, orbital hybridization mechanisms, and mechanical performance properties) of oxygen deficit perovskite-based cuprate Type-II superconductors.

2.1.1 Structure of YBCO System

The structure of yttrium rare earth-containing type-II (YBCO) superconducting system, the first material exhibiting a transition temperature value higher than the boiling point of liquid nitrogen, has been crystallized in the orthorhombic P_{mmm} symmetry and has been observed to obtain the oxygen deficit multi-layered perovskite structure derived from the ideal perovskite structure depending on the intergrowth of adjacent layers and/or the removal of oxygen atoms from the crystal system [56]. The YBCO parents are composed of four main participants with respect to the CuO_2 planes and Cu-O chain numbers in a unit cell: namely, Y-358, Y-124, Y-247, and Y-123 superconducting phases. Thus, the parents possess a wide range of characteristic features. Here, the latter superconducting phase (stoichiometrically $YBa_2Cu_3O_{7-y}$) obtaining one Cu-O chain and two Cu-O_2 layers in its crystal structure exhibits the highest transition temperature of 92- 94 K [57]. Besides, the $YBa_2Cu_3O_{7-y}$ superconductor has contained both the Cu-O layers in the *ab* plane and Cu–O chains in the *b*-axis in the multilayered crystal structure. The main difference between the other high temperature superconductors (oxygen deficit perovskite-based Tl-parents, Hg-parents, and Bi-parents) is the presence of antiferromagnetic Cu–O chains in the *b*-axis. In more detail, the strongly covalently bonded Cu–O ribbons have been surrounded with 4 oxygen atoms along the *a*-axis (defined as O-1 sites) and *b*-axis (termed as O-5 sites) of orthorhombic crystal structure. In the crystal system, the former sites are occupied fully whereas the latter sites are unoccupied. Correspondingly, the occupation of the O-1 and O-5 sites determines the lengths of *a* and*b*-axes. That is, the full occupation triggers the enlargement of the b-axis, on this basis the length of the b-axis is a little larger as compared to the length of the *a*-axis in an orthorhombic crystal structure [50]. Additionally, the Cu-O layers have been surrounded with 5 oxygen atoms located along the *a*-axis (defined as O-2 sites) and *b*-axis (termed as O-3 sites) in the 3D polyhedron shape geometry [49]. The formation of Cu-O ribbons and Cu-O layers in the crystal system stems from the interconnection of Y-CuO-BaO-CuO_2-BaO-CuO_{2-Y} layers [48]. The antiferromagnetic Cu-O layers in the crystal system are in charge of conduction mechanism of $YBa_2Cu_3O_{7-y}$ superconductor. At the same time, the Cu-O ribbons are used to be the charge reservoirs for the formation of mobile holecarriers in the weakly coupled copper-oxide layers. Thus, the variation of oxygen content in the

Cu-O chains affects seriously the superconductivity phenomenon. In more detail, alteration in the oxygen state of O-1 sites (depending on the material preparation conditions, purity level, dopant type, addition, and substitution mechanism) changes not only the crystallization symmetry and superconducting features of $YBa_2Cu_3O_{7-y}$ superconductor. As for the other layers related to the yttrium (Y) and barium (Ba) sites in the crystal system, the barium planes locate between the strongly covalently bonded Cu–O ribbons and Cu-O planes in the unit cell of $YBa_2Cu_3O_{7-y}$ crystal system, and the related oxygen sites in the Ba-O are termed as O-4 sites. Moreover, the yttrium sites (free-oxygen sites) locate between the Cu-O planes (where the conductivity mechanism takes place) in the system. This is exactly substitution of yttrium for the cations/anions in the $YBa_2Cu_3O_{7-y}$ system triggers the considerable differentiation in the superconductivity phenomenon than that of barium sites as a consequence of the location regions. Thus, the addition or substitution mechanism for the Ba-sites plays the minimum active role in the drive of superconductivity phenomenon. However, regardless the partial substitution in the antiferromagnetic Cu–O ribbons and Cu-O planes in the $YBa_2Cu_3O_{7-y}$ crystal system much more affects the fundamental characteristic features including electrical, flux pinning ability, morphological, crystallinity quality, grain boundary couplings, structural, and mechanical performance properties as compared to the cationic substitution by outside the Cu-sites. Namely, any cationic substitution in the Cu–O ribbons and Cu-O planes leads remarkably the degradation in the basic characteristics of $YBa_2Cu_3O_{7-y}$ system due to the suppression of Cu-O coordination, stabilization of structure, formation of orbital hybrids, carrier concentrations, antiferromagnetic spin fluctuation, spin-density wave systems, percolative paths, bond distances of Cu-O planes, orbital hybridization mechanism, and copper oxidation states. Additionally, it should be added that the reduction in the oxygen content in the unit cells with the addition/substitution mechanism is known to damage dramatically the superconductivity phenomenon because of the susceptibility to oxygen deficiency of $YBa_2Cu_3O_{7-y}$ superconductor. This is because the considerable decrement trend in the oxygen content level causes the crucial following results:

1- occupation of O-5 sites in the *a*-axis in the Cu-O ribbons (change in the homogeneities of oxidation states),

2- decrease of the main oxygen level in the O-1 sites along the *b*-axis in the antiferromagnetic Cu–O chains,
3- beginning of phase transition from orthorhombic phase to tetragonal phase (O–T transition),
4- change in the crystallization activation energy,
5- rearrangement of the Cu-O coordination polyhedra and Ba-O bonds, (can also be observed for the replacement of cations in yttrium sites)
6-formation of the double chain layers with additional Cu-O chains adjacent to Ba-O planes,
7- increase in the impurity phases,
8- decrease in the characteristic $YBa_2Cu_3O_{7-y}$ superconducting phase,
9-variation in the phase coherence and amplitude of the pair wave function [58–60].
On the other hand, any cationic substitution by the Ba sites and especially Y sites (closest points to the antiferromagnetic Cu-O layers) may enhance in the characteristic features mentioned above as a result of the change in the thermodynamic stability, surface nucleation growths, ionization potential, electron affinity, chemical potential, electrophilicity, charge transfer index (charge reservoir regions), chemical stability, oxygen content level, new bond (chemical or ionic) formations, re- modification of skeleton layers, crystallization reaction kinetics,atomic disorders, re-ordering of geometrical structures, vibrational frequencies of pure $YBa_2Cu_3O_{7-y}$ superconductors [61–66]. Accordingly, the differentiation of the main characteristic properties (namely, electronegativity, valance electron states, electron configurations, cation-vacancy, ionic radius dimensions, atomic occupancy ratios, magnetic moment magnitude) between the addition or substitution atoms and host atoms in the crystal sites is the main reason for the improvement in the fundamental characteristic features [61–70]. Additionally, the formation on non-recoverable microscopic problems in the main $YBa_2Cu_3O_{7-y}$ matrix with the addition or substitution mechanism is another probable effect on the alteration in thebasic characteristics of $YBa_2Cu_3O_{7-y}$ superconductor. Hence, the studies related to any cationic/anionic substitution for outside the Cu-O_2 layers and Cu-O chains is a subject worth studying.

3. MATERIALS AND METHODS

3.1 $YBa_2Cu_3O_{7-y}$ Superconductor Preparation Procedure

In the present study, the role of oxygen and Mn2O3 impurity roles on the basic characteristic features electrical, flux pinning ability, stabilization of system, morphological, pairing mechanism, crystallinity quality, grain boundary couplings, structural, orbital hybridization mechanisms, and superconducting properties of $YBa_2Cu_3O_{7-y}$ superconductors. In this respect, this study is composed of four main preparation procedures: (I) production of the pure $YBa_2Cu_3O_{7-y}$ superconductors in the bulk formations under oxygen and oxygen-free annealing ambient conditions, (II) determination of optimum annealing ambient for the $YBa_2Cu_3O_{7-y}$ superconducting phase, (III) preparation of bulk $YBa_2Cu_3O_{7-y}$ superconductor with different Mn_2O_3 impurity addition amounts ($0.00 \leq x \leq 0.30$) under the oxygen and oxygen-free annealing ambient conditions, and (IV) and detection of the optimum manganese addition amount for the formation of highest $YBa_2Cu_3O_{7-y}$ superconducting phase in the crystal structure. For this aim, initially the pure $YBa_2Cu_3O_{7-y}$ superconductors in the bulk formations have been produced by conventional ceramic method**.** The chemical components (Y_2O_3, $BaCO_3$, CuO, Mn_2O_3 powders) within the high purity of about 99.99% have been obtained from Alfa Aesar exclusive distributor (Picture 3.1). Then, the powders of chemicals have been weighed to be 4mg in total in a mole-to-mole ratio of 1:2:3 (traditional Y-123 superconducting phase) by using an electronic balance in the atmospheric air conditions (Picture 3.2). The powders of chemicals have been exposed to the mixing process in a grinding machine for 9 h in the medium of air to provide a reduction to the desired size of powder particles and increase the homogeneity of the chemical mixture (Picture 3.2). The homogenous mixture of powder chemicals has manually been ground in an agate mortar for about half an hour so that the chemical particles have been brought closer together as much as possible to strengthen the interparticle (chemical or ionic) bonds with each other. The resultant form of chemicals placed into the porcelain crucibles has thoroughly been subjected to the pre-heating process at 930 °C for 36 h under 3 °C/min heating rate in a conventional ashing furnace (Picture 3.2). Similarly, the material preparation ambient temperature in the furnace has been decreased with the 3 ºC/min cooling rate to the room temperature. The calcination process has been applied to remove any residues related the carbon or carbon-containing impurity from the homogenously mixed chemicals. Thus, we have gathered the stoichiometrically $Y_1Ba_2Cu_3O_{7-y}$ powder as requested. The resultant chemicals have been taken from the ashing furnace and it has been determined that the color of the chemicals has turned blackish color. The last form of powder mixture has been re-milled in the agate mortar for the duration of 30 min using a grinding pestle to increase the homogeneity, intermolecular bonding and to achieve the optimum size of chemicals particles [71]. Afterward, the calcined powders have been pelletized into the rectangular bars with the size of 2.0x0.5x0.2 cm^3 in medium of atmospheric air not only to strengthen the grain boundary couplings between the adjacent layers, but also to overcome the intergrain connections and non-recoverable microscopic problems in the main $YBa_2Cu_3O_{7-y}$matrix (Picture 3.2). Then, the pelletized bars have been annealed at 945 °C for 24 h in the atmospheric air. The heating rate has been adjusted as 3 °C/min as the calcination process. After 24-h heat treatment, the temperature has been decreased by 1 °C/min cooling rate down to the value of 720 °C. After this point, we have used two different methods: production of the pure $YBa_2Cu_3O_{7-y}$ superconductors in the bulk formations (i) oxygen-free and (ii) oxygen annealing ambient conditions. For the first part, the annealing procedure with the heating rate of 1 °C/min has continued towards the room temperature. As for the second step, the oxygen gas has flowed in the annealing ambient (with the same heating rate of 1 °C/min) until 400 °C temperature value to recover the oxygen lost to $YBa_2Cu_3O_{7-y}$ superconductor due to the heating processes and provide the main $YBa_2Cu_3O_{7-y}$ superconducting phase in the crystal structure [72]. Accordingly, we have determined the optimum annealing ambient for the $YBa_2Cu_3O_{7-y}$ superconducting phase. For the third and fourth stages (manganese addition procedures and annealing under the oxygen and oxygen-free annealing ambient conditions), we have begun the mixing process with the presence of different Mn_2O_3 impurity addition amounts ($0.00 \leq x \leq 0.30$) and thus followed the same procedures. Moreover, we should declare that all values (calcination/annealing time and temperature, oxygen flow rate, palletization load and duration) used in this study are taken from optimum material preparation processes in the literature. The bulk $YBa_2Cu_3O_{7-y}$ superconductors prepared with different Mn impurity addition levels such as 0, 0.01, 0.03, 0.05, 0.07, 0.10, and 0.30 have thereafter been presented to be pure, Mn-1, Mn-2, Mn-3, Mn-4, Mn-5, and Mn-6 superconductors, respectively. Besides, the bulk $YBa_2Cu_3O_{7-y}$ superconductors prepared under oxygen annealing ambient conditions have been pointed out by the letter of O. Namely, the superconducting samples prepared with different Mn impurity addition levels ($0.01 \leq x \leq 0.30$) under oxygen ambient have thenceforth been presented to be OMn-1, OMn-2, OMn-3, OMn-4, OMn-5, and OMn-6 superconductors, respectively.

Picture 3.1: YBCO from Alfa Aesar exclusive distributor, the high purity of about 99.99%

Picture 3. 2: Measuring devices used in sample preparation.

3.2 Experimental Methods for Measurements

The effect of oxygen and Mn_2O_3 impurity addition amounts roles (0.01≤x≤0.30) on the basic characteristic features electrical, flux pinning ability, stabilization of system, morphological, pairing mechanism, crystallinity quality, grain boundary couplings, structural, orbital hybridization mechanisms, and superconducting properties of polycrystallized $YBa_2Cu_3O_{7-y}Mn_x$ superconductors by means of electrical resistivity (ρ-T), X-ray diffraction (XRD), critical current density (I-V), scanning electron microscopy (SEM), and related theoretical results.

3.2.1 Electrical Resistivity Tests

The general electrical resistivities of pure and Mn added bulk $YBa_2Cu_3O_{7-y}$ superconductors have been inspected considering the standard four-point contact (Picture 3.3) measurements in a cyclic cryogenic refrigeration system (Picture 3.4). The contacts have been made with highly conductive silver paint to minimize contact contribution to the residual resistivity parameter. Regardless, in the measurements the contact resistance can be observed. Throughout the electrical tests, 5 mA dc current has been applied to the surface of sample, and dc electrical resistivity signals have been measured using a programmable nano-voltmeter and current source in the temperature ranges from 30 K to 300 K. The accuracy has been detected to be about ±0.1 K. Besides, the experimental results for the electrical resistivity measurements have enabled us to discuss the effect of oxygen and Mn_2O_3 impurity addition on the normal state electrical resistivities (ρ_{300K}), hole carrier concentrations (P_{hole}), offset/onset transition temperatures (T_c^{offset} and T_c^{onset}), residual resistivity (ρ_{res}), residual resistivity ratio ($RRR = \rho_{90K}/\rho_{300K}$), degree of broadening ($\Delta T_c = T_c^{onset} - T_c^{offset}$),$\rho_{100K}$, ρ_{norm}, and $\Delta\rho$. We have also examined the variation of polaronic states, stabilization of structure, formation of orbital hybrids, spin-density wave systems, surface nucleation growths, re-ordering of Cu-O bonds, antiferromagnetic spin fluctuation, superconducting energy gaps, percolative paths, copper oxidation states, and orbital hybridization (overlapping) mechanisms of bulk $YBa_2Cu_3O_{7-y}$ superconductors depending on both the oxygen and Mn_2O_3 impurity addition.

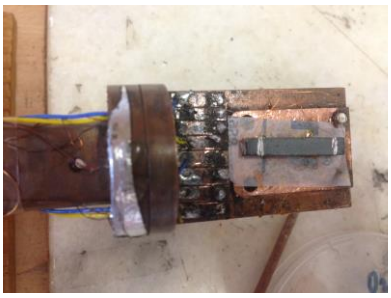

Picture 3. 3: Experimental set up for the 4-point probe measurement.

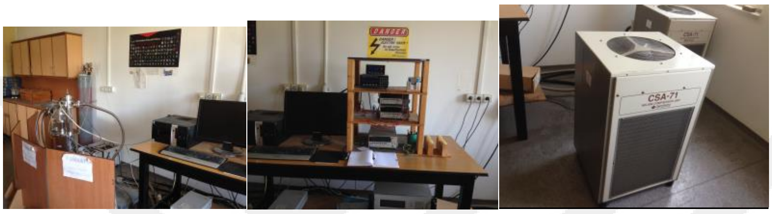

Picture 3. 4: Cyclic cryogenic refrigeration system.

3.2.2 X-Ray Diffraction Measurements

The variations of crystalline structure (phase volume fractions, crystallinity quality, crystallization system, lattice cell constant parameters, thermodynamic stability, grain (mis)alignments, reaction kinetics, oxygen ordering degree in the short-range ordered antiferromagnetic Cu-O chains, orthorhombic distortion, oxygen concentrations in unit cells, grain alignment distributions and orientations, lattice strains, dislocation densities, phase transition from orthorhombic phase to tetragonal phase, surface nucleation and growth mechanisms) of $YBa_2Cu_3O_{7-y}$ superconductors with the oxygen and Mn_2O_3 impurity addition amounts have been investigated by using characteristic peak reflection intensities in the XRD diffractograms (Picture 3.5). The XRD spectra have been gathered with the aid of a Rigaku Multiflex diffractometer that emits X-rays with the wavelength of 1.54 Å at the powers of 26 mA and 36 kV. The XRD patterns have been recorded between the 2Θ angles of 5° and 65° at a scan speed of 3.0°/min at the room temperature in the air atmosphere. The XRD pattern signals have been monitored by a well-equipped computer.

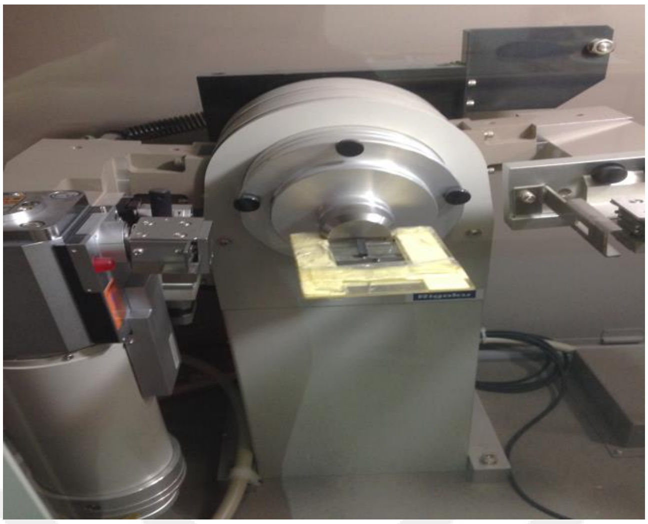

Picture 3. 5: X-ray diffractometer system.

3.2.3 SEM Experimental Measurements

In the current work, the scanning electron microscopy (SEM) examination has been used to determine the role of oxygen and Mn_2O_3 impurity on the alteration of view of surface morphology, crystal structure quality, microcrystal coalescence orientations, granular structure, grain alignment distributions and orientations, particle growth distributions, structural changes, internal defects, porosity, microvoids, intragrain and inter-grain boundary couplings, and non-recoverable microscopic problems of pure and Mn added bulk $YBa_2Cu_3O_{7-y}$superconductors have been examined in detail. The SEM investigations have been performed by Jeol JSM 5600 SEM device under 20 kV external voltages at x5000 magnification.

3.2.4 Transport Critical Current Density Measurements

The change in the critical current carrying ability based on the self-field transport current density measurements of bulk $YBa_2Cu_3O_{7-y}$ superconductors with the oxygen and Mn_2O_3 impurity has been researched by using the variation of voltage parameters as a function of applied currents (I-V tests). The tests have been conducted with the aid of the four-probe contact method in the home-made system at liquid nitrogen temperature without any magnetic field. The experimental findings for the current density have been determined from the standard criterion value of 1 μV/cm. The critical current density parameters have enabled us to discuss the role of oxygen and Mn_2O_3 impurity on the numbers of flux pinning centers, flux pinning ability, energy barriers, strength of coupled vortices, elasticity of nucleation mechanism, vortex lattice period, grain boundary couplings, and motions of thermal flux on vortices in 2D pancake vortices in the $YBa_2Cu_3O_{7-y}$ system.

4. RESULTS AND DISCUSSION

4.1 Change of General Resistivities Grounded on Dc Electrical Experiments

The differentiation of basic electrical quantities (normal state electrical resistivities, residual resistivity, residual resistivity ratios, ρ_{100K}, ρ_{norm}, and $\Delta\rho$ and superconducting properties (offset/onset transition temperatures, degree of broadening transitions, and charge carrier concentrations in the valence bands) of bulk $YBa_2Cu_3O_{7-y}$ superconductors with the oxygen and different Mn_2O_3 impurity addition has been examined by using the temperature-dependent electrical resistivity experiments performed in the temperature range of 25 K-110 K to bring out a relationship between the basic electrical quantities and microscopic structural problems. The experimental curves for all the samples have been depicted in Figure 4.1 (pure and Mn added bulk $YBa_2Cu_3O_{7-y}$superconductors prepared at without the oxygen ambient condition) and Figure 4.2 (pure and Mn added $YBa_2Cu_3O_{7-y}$ superconductors produced under the oxygen ambient condition). This part of the paper has been focused sensitively on electrical resistivity parameters. It has been clear from the figures that both the oxygen and Mn_2O_3 impurity addition amount has triggered serious differentiations on the fundamental electrical resistivities of multi-layered perovskite $YBa_2Cu_3O_{7-y}$ superconductors. On this basis, the variations of electrical properties with the oxygen annealing ambient conditions have stemmed from the oxygen annealing ambient has re-organized the Cu-O coordination, stabilization of structure, homogeneities of oxidation states, antiferromagnetic spin fluctuation (weak coupling theory) in the Cu–O chains, bond distances of Cu-O planes, and superconducting phases due to the change in the orthorhombicity and oxygen ordering degree in the strongly covalently bonded Cu-O_2 layers. Similarly, the differentiation of the basic electrical quantities with the increase in the Mn_2O_3 impurity addition amount in the $YBa_2Cu_3O_{7-y}$ superconductors has confirmed that the foreign impurity has successfully been introduced in the crystal system. As for the detailed discussions for the electrical resistivity parameters, all the pure and $YBa_2Cu_3O_{7-y}Mn_x$ superconductors (except for the bulk OMn-6 sample) have presented the standard metallic characteristics (linear dependence of resistivity over temperature, dρ/dt) above transition temperatures as a result of the logarithmic change in electronic density states at the Fermi level [73–75]. Likewise, according to the weak coupling theory, the linear variation in the electrical resistivity curves has stemmed from the existence of pairing mechanism (meaning the interactions between electron-electron and electron-phonon for the formation of super-electrons and cooper-pairs) for antiferromagnetic spin fluctuations in the microdomain clusters of the $YBa_2Cu_3O_{7-y}$ system [76, 77]. Further, the liquid model has showed that the separation of electron spin charges in the weakly coupled Cu-O_2 layers has been charge of the phase transition from the metal to the superconductivity since relaxation rate belonging to the longitudinal transport has equaled $1/\tau \sim T$ [78, 79]. On the other hand, the excess manganese impurity addition has resulted in the semiconducting behavior for the OMn-6 superconducting compound as a result of metal to insulator transition (MIT) [80]. Besides, the change in the metallic characteristic behavior with the oxygen ambient and Mn_2O_3 impurity has resulted from the differentiation in the number of charge carrier concentrations in the in-plane Cu-O bonds [81, 82]. Additionally, the variations in the non-recoverable microscopic structural problems related to the structural changes, stress raisers, internal defects, microcrystal coalescence misorientations, porosity, microvoids, intragrain and inter-grain boundary couplings between adjacent layers are responsible for the metallic behavior of $YBa_2Cu_3O_{7-y}$ crystal system [83]. According to the experiments, both the oxygen ambient and the presence of optimum Mn_2O_3 impurity have led not only to the improvement in the charge carrier numbers and couplings between adjacent superconductive layers but to decrease in the non-recoverable microscopic structural problems, as well [84–87]. Conversely, as performed in any experimental studies the presence of excess Mn_2O_3 impurity in the $YBa_2Cu_3O_{7-y}$ crystal system has damaged considerably the main electrical and superconducting mechanism in the system due to the reorganization of Cu-O coordination and degradation in the stabilization of skeleton structure, homogeneities of oxidation states, couplings between adjacent superconductive layers, and stabilization of orthorhombic P_{mmm} symmetry [88-90]. Besides, the charge carrier concentrations have been observed to diverge seriously from the optimum number for the typical $YBa_2Cu_3O_{7-y}$ system [91, 92]. To point out which annealing ambient conditions are optimum for supporting the basic electrical conductivity properties for the bulk $YBa_2Cu_3O_{7-y}$ superconductors we have compared the experimental electrical resistivity curves for two pure samples prepared at oxygen and oxygen-free annealing ambient in Figure 4.3. It has been obtained from the figure that the preparation conditions including oxygen ambient have made the pure $YBa_2Cu_3O_{7-y}$ superconductor present much superior electrical conductivity features. On this respect, we have hereafter dwelled on the materials prepared in the presence of oxygen ambient more. Thus, one can see the room temperature electrical resistivity (ρ_{300K}), residual resistivity (ρ_{res}), residual resistivity ratio ($RRR = \rho_{100K}/\rho_{300K}$),$\rho_{100K}$, ρ_{norm}, and $\Delta\rho$ parameters deduced from the electrical resistivity curves in Table 4.1 (oxygen-free ambient) and Table 4.2 (with oxygen ambient). Initially, both Table have displayed that all the parameters have been found to change drastically depending on the oxygen ambient and Mn_2O_3 impurity addition level. If going back to Figure4.3 for the comparison of data belonging to the pure samples, the $YBa_2Cu_3O_{7-y}$ superconductor produced without oxygen has possessed the relatively higher room temperature resistivity value of 77.713 mΩ.cm as compared to that (21.005 mΩ.cm) of $YBa_2Cu_3O_{7-y}$ superconductor produced at the oxygen ambient. Similarly, the ρ_{res} parameters have been found to be about 16.870 mΩ.cm and 5.974 mΩ.cm for the pre and pure samples, respectively. One can encounter all the resistivities in Table 4.1 and Table 4.2. Based on the electrical results, it is obvious that the presence of the oxygen in the material production process have encouraged the pure $YBa_2Cu_3O_{7-y}$ sample to exhibit more superior electrical conductivity. Thus, we have thenceforward discussed the variation in the basic electrical resistivities for only the $YBa_2Cu_3O_{7-y}$ superconductor produced with oxygen ambient condition due to the superior electrical conductivity features. It has been observed from Table 4.2, with the increase in the manganese addition amount in the $YBa_2Cu_3O_{7-y}$ superconductor up to the certain value the basic electrical characteristics have been noted to improve seriously. In more detail, the normal state electrical resistivity values at room temperature have been found to decrease with the increase in the Mn addition amount up to x=0.07 beyond which the ρ_{300K} parameters have been found to increase again. Numerically, the pure sample has had the ρ_{300K} value of 21.005 mΩ.cm whereas the minimum value of 12.975 mΩ.cm has been recorded for the OMn-4 sample. Contrariwise, the highest ρ_{300K} value of 139.555 mΩ.cm has been measured for the OMn-6 superconductor. As for the oxygen-free heating process results, although the ρ_{300K}values have been observed to vary randomly with respect to the manganese impurity addition amount (it is of course we should not ignore the positive resistivity contribution of silver contacts), the maximum highest ρ_{300K} value of 192.370 mΩ.cm has been recorded for the Mn-6 sample. This points clearly out that the presence of excess manganese impurity has caused the significant increase in the ρ_{300K} value due to the formation of non-recoverable microscopic structural problems in the $YBa_2Cu_3O_{7-y}$ superconductor and divergence of charge carrier concentrations from the optimum numbers in the conduction Cu-O_2 layers [93]. On the other hand, the optimum manganese impurity addition level of x=0.07 has also improved the crystal structure quality and pairing mechanism.

As for the change in the electrical parameter of temperature-independent residual resistivities evaluated from Matthiessen's rule (based on the extrapolation technique on the resistivity findings) for the pure and Mn-added $YBa_2Cu_3O_{7-y}$ superconductors prepared under the oxygen annealing ambient conditions, both the oxygen and manganese addition in the crystal system have seriously affected the ρ_{res} parameters related to directly non-recoverable microscopic structural problems, crystallinity quality, grain boundary couplings (metallic interactions) between the adjacent layers in thebulk $YBa_2Cu_3O_{7-y}$ crystal system [94].

In this context, the optimum Mn impurity addition level of x=0.07 has developed the crystallinity quality of $YBa_2Cu_3O_{7-y}$ superconductor as a consequence of the elimination of microscopic structural problems. On the other hand, the excess manganese has triggered the permanent microscopic structural problems, grain misalignment distributions and misorientationsfor the degradation in the crystallinity quality of $YBa_2Cu_3O_{7-y}$ system. Numerically, the minimum temperature-independent residual resistivity parameter has been found to be about 0.304 mΩ.cm for the bulk OMn-4 superconductor whereas the maximum ρ_{res}value of about 125.116 mΩ.cm for the bulk OMn-6 samples. The other Mn-added $YBa_2Cu_3O_{7-y}$superconductors have exhibited the moderate ρ_{res} values including 5.974 mΩ.cm for the pure sample, 5.782 mΩ.cm for the OMn-1 compound, 3.125 mΩ.cm for the OMn-2 superconducting sample, 2.966 mΩ.cm for the OMn-3 material, and 5.782 mΩ.cm for the OMn-5 compound. Correspondingly, the breaking point for the temperature-independent residual resistivity parameter has been noted to be x=0.10.

Moreover, the electrical resistivity curves at the vicinity at 100 K (ρ_{100K}) belonging to the pure and Mn added $YBa_2Cu_3O_{7-y}$ superconductors have enabled us to evaluate the variation (new introductions or decreases) in the lattice strain fields, amplification (stress concentration) sites, and impurity scatterings in the crystal system. Here, the value of 100 K is directly related to the transition between the normal state and superconducting state for the transcrystalline regions in the isolated grains and a symbolic value [95]. According to Table 4.2, the ρ_{100K} parameters have been noted to decrease constantly from the 9.871 mΩ.cm (for the pure sample) to 1.182 mΩ.cm (for the bulk OMn-4 superconductor) depending on the manganese impurity addition level up to x=0.07 above which the parameters have been found to increase immediately and reached the maximum value of 167.979 mΩ.cm for the bulk OMn-6 superconductor. Accordingly, the experimental findings for the ρ_{100K} parameters have shown that among the materials studied, the OMn-4 superconductor has presented the best crystallinity quality because of the decrease in the lattice strain fields, stress concentration sites, and impurity scatterings in the crystal system. All the experimental findings have already been favored completely by the other parts.

We have also determined the residual resistivity ratios (abbreviated as RRR=ρ_{300K}/ρ_{100K}) related to the material quality for every material studied in the current work. One can see the effect of oxygen and different manganese addition impurity amounts on the RRR parameters in Table 4.1 and Table 4.2. However, as mentioned above, we have examined in detail the role of Mn_2O_3 impurity on the $YBa_2Cu_3O_{7-y}$ superconductors prepared under oxygen annealing ambient conditions. It has been observed from Table 4.2 that up to the critical manganese impurity addition level of x=0.5 the value of RRR parameter has been found to be between 2.123 (for the pure sample)-2.430 (for the bulk OMn-3 superconductor). After this critical ratio, there has been a serious jump in the RRR parameter toward the value of 10.977. There are two main reasons for the considerable increment. The first one is that the OMn-4 sample with relatively higher transition temperature value than 100K has exhibited the superconducting behavior. Namely, the ρ_{100K} parameter has coincided with the point of increase in resistivity, and can be sifted to higher values such as 100K. However, there would be conflict with other values. The second one is related to the fact that the OMn-4 sample has the best pairing mechanism, especially crystallinity quality with rather fewer microscopic structural problems and grain boundary couplings between the adjacent layers as we have discussed before. In other words, the optimum manganese impurity encourages the $YBa_2Cu_3O_{7-y}$ superconductors to use in the application fields[96].

The other electrical resistivity parameter of $\Delta\rho$ computed by subtracting two ρ_{100K} and ρ_{300K} parameter has been used to determine the influence of manganese impurity addition on the internal defects, porosity, microvoids, intragrain and inter-grain boundary couplings in the $YBa_2Cu_3O_{7-y}$ superconductors. This parameter is also used to define the main electrical behavior (metallic or semiconducting) of a material. In the current work, one can encounter the differentiations in the $\Delta\rho$ parameters for the pure and Mn-added perovskite-based $YBa_2Cu_3O_{7-y}$ cuprate superconductors produced under oxygen ambient and without oxygen ambient conditions in Table 4.1 and Table 4.2. Because of more outstanding features of the former group, we have only discussed the change in the $\Delta\rho$ parameters of the materials prepared at oxygen ambient condition. On this basis, Table 4.2 has shown that the values of $\Delta\rho$ parameter have been found to be approximately between 8-13 mΩ.cm for the pure, OMn-1, OMn-2, OMn-3, OMn-4, and OMn-5 superconducting samples. On the other hand, the bulk OMn-6 sample has ben noted to present the negative $\Delta\rho$ parameter due to the semiconducting behavior depending on the metal to insulator transition (MIT). The $\Delta\rho$ parameter should be evaluated with the ρ_{norm} parameter when comparing the crystal structure quality between the superconducting compounds. Hence, we have also been interested in the ρ_{norm} parameter that is deduced from the direct relation between the ρ_{100} and $\Delta\rho$ values and is related to the temperature-dependent region in the resistivity curves. Accordingly, the ρ_{norm} parameter (including the combination of $\Delta\rho$ parameter) can be used to discuss the differentiation in the crystal structure quality, microscopic structural problems, and grain boundary couplings between the adjacent multilayers [97,98].The experimental findings have shown that with the increase in the manganese impurity addition amount in the crystal lattice, the ρ_{norm} parameter has been recorded to decrease, and in fact the minimum ρ_{norm} parameter has been noted to be about 0.100 for the optimum Mn added OMn-4 superconducting sample. Beyond the critical addition level, there has appeared a rapid increase in the ρ_{norm}

parameter to the value of 1.790 (Table 4.2). On the other hand, the OMn-6 superconducting sample with highest manganese impurity in the crystal structure has presented ρ_{norm} value of -5.910 (due to the semiconducting behavior). Additionally, the numerical values have declared that the existence optimum manganese impurity (x=0.07) in the $YBa_2Cu_3O_{7-y}Mn_x$ crystal system prepared at the oxygen annealing ambient has led the improvement in the crystallinity quality and paring mechanism. Contrarily, the excess Mn impurity has found to damage considerably the basic resistivity characteristics and crystallinity quality of $YBa_2Cu_3O_{7-y}$ superconductors. Resistivity measurements show that the presence of manganese in the $YBa_2Cu_3O_{7-y}$ superconductors has enabled us to determine by means of the change in the oxygen content levels (if the manganese causes the production of less (well) oxygenated $YBa_2Cu_3O_{7-y}$ samples, the change of c-axis resistivity is the semiconducting (the linear) dependence) in the main crystal matrix.

Table 4. 1: Electrical resistivity parameters oxygen Free ambient.

Samples	ρ_{300K} (mΩcm)	ρ_{res} (mΩcm)	RRR (ρ_{300K}/ρ_{100K})	$\Delta\rho$ ($\rho_{300K}-\rho_{100K}$) (mΩcm)	ρ_{norm}($\rho_{100}/\Delta\rho$)	P_{100K} (mΩcm)	T_c^{onset} (K)	T_c^{offset} (K)	ΔT_c (K)
Pure	77.713	16.870	2.583	44.534	0.745026	33.179	87.651	92.497	4.846
Mn-1	49.993	0.915	5.811	37.948	0.317408	12.045	88.953	92.634	3.681
Mn-2	47.764	1.898	4.724	41.252	0.157859	6.512	85.980	89.893	3.913
Mn-3	44.697	2.154	4.497	35.206	0.269585	9.491	83.241	87.885	4.644
Mn-4	47.658	3.294	3.203	32.777	0.454007	14.881	82.556	87.708	5.152
Mn-5	42.921	4.442	3.173	30.025	0.429509	12.896	82.205	88.900	6.695
Mn-6	192.370	118.639	1.369	51.805	2.713348	140.565	53.094	81.562	28.468

Table 4. 2: Electrical Resistivity Parameters with Oxygen Ambient.

Samples	ρ_{300K} (mΩcm)	ρ_{res} (mΩcm)	RRR (ρ_{300K}/ρ_{100K})	$\Delta\rho$ ($\rho_{300K}-\rho_{100K}$) (mΩcm)	ρ_{norm}($\rho_{100}/\Delta\rho$)	ρ_{100K} (mΩcm)	T_c^{onset} (K)	T_c^{offset} (K)	ΔT_c (K)
Pure	21.005	5.974	2.123	11.134	0.887	9.871	92.816	94.282	1.466
OMn-1	22.110	5.782	2.350	12.7	0.7401	9.410	94.202	96.084	1.882
OMn-2	15.256	3.125	2.343	8.744	0.745	6.512	94.662	96.923	2.261
OMn-3	13.451	2.966	2.430	7.916	0.699	5.535	96.340	97.303	0.963
OMn-4	12.975	0.304	10.977	11.793	0.100	1.182	98.320	100.504	2.184
OMn-5	31.072	5.782	1.559	11.137	1.790	19.935	91.262	94.873	3.611
OMn-6	139.555	125.116	0.831	-28.424	-5.910	167.979	47.304	72.638	25.334

4.1.1 Evolution of Superconducting Quantities of Bulk $YBa_2Cu_3O_{7-y}$ Superconductors with Manganese Impurity and Oxygen Ambient

In this part, the variation of superconducting properties including the offset/onset transition temperatures (T_c^{onset} / T_c^{offset}), degree of broadening transitions (ΔT_c), and charge carrier (P) concentrations in the valence bands ofperovskite-based YBa2Cu3O7-y cuprate superconductors with the oxygen annealing ambient condition and different manganese impurity addition amount has been studied by means of the standard temperature-dependent resistivity experiments exerted in the temperature range between 25 K and 110 K. The observed parameters have numerically been depicted in Table 4.1 (including the experimental results for the pure and Mn-added YBa2Cu3O7-y cuprate superconductors prepared without the oxygen ambient condition) and Table 4.2 (including the results for the YBa2Cu3O7-y superconductors produced under the oxygen ambient condition). The T_c^{offset} transition temperature is directly associated with the pairing mechanismor polaronic effect (electron-electron and electron-phonon interactions = formation of super-electrons and cooper-pairs) for antiferromagnetic spin fluctuations in the microdomain clusters of the YBa2Cu3O7-y system [99]. Thus, the T_c^{offset} indicates the phase transition between the normal state and superconducting state for both the inter-granular areas and transcrystalline regions in the isolated grains [100]. Correspondingly, the T_c^{offset} value is seriously affected by the formation of any impurity phases in the crystal system. As for the T_c^{onset} parameter, the superconducting phase transition becomes for only the transcrystalline regions of YBa2Cu3O7-y system. Besides, the T_c^{onset} parameter is used to define some important parameters; namely, formation of electron-electron and electron-phonon interactions, pair binding energy, order parameter for the super-electrons and cooper-pairs, formation of bipolarons in the polarizable lattices, phase coherence and amplitude of the pair wave function, overlapping mechanism, localization for the electronic densities of states (DOS), organization of the Cu-O coordination, homogeneities of oxidation states, microscopic structural problems, and grain boundary couplings between the adjacent layers in quantum mechanical, basic physical and thermodynamics fields [101,102]. According to Figure 4.1 and Figure 4.2, the presence of both the oxygen in the material production process and manganese impurity in the crystal system has considerably damaged the superconducting properties of $YBa_2Cu_3O_{7-y}$ superconductors. It has been apparent from Table 4.1 and Table 4.2 that the pure $YBa_2Cu_3O_{7-y}$ sample prepared without oxygen ambient condition has obtained the T_c^{onset} and T_c^{offset} values of 87.651 K and 92.497 K, respectively. In the case of oxygen in the material production process, the pure superconductor has exhibited the T_c^{onset} and T_c^{offset} values of 92.816 K and 94.282 K. Similarly, the existence of oxygen has caused the enhancement in the transition temperature parameters belonging to the $YBa_2Cu_3O_{7-y}$ sample. Therefore, we have discussed the change of the superconducting features mentioned above for only the manganese added $YBa_2Cu_3O_{7-y}$ superconductors prepared under the oxygen annealing ambient conditions. In this context, Table 4.2 has shown that both the values of T_c^{onset} and T_c^{offset} parameters have been found to increase systematically with the manganese impurity addition ratio up to x=0.07 where the OM-4 superconducting sample has had the highest T_c^{onset} and T_c^{offset} values of 98.320 K and 100.504 K. Conversely, the presence of excess manganese impurity in the system has decreased the T_c^{onset} and T_c^{offset} values towards 47.304 K and 72.638 K, respectively. This is because the addition of optimum manganese impurity has organized the Cu-O coordination and stabilized the crystal structure as much as possible. Besides, the oxygen-free annealing ambient and excess manganese impurity has led to re-order the interconnections of Y-CuO-BaO-CuO_2-BaO-CuO_2-Y layers due to the varied valence electron states, ionic radius dimensions, and electronegativity of Mn^{+3} and host ions in the $YBa_2Cu_3O_{7-y}$ superconducting system. Correspondingly, the local differentiation in the main matrix has weakened the charge carriers transfer depending on the degradation in the Cu-O_2 interlayer coupling strengths [101,102,104,105]. Further, the pairing mechanism for antiferromagnetic spin fluctuations in the microdomain clusters of the$YBa_2Cu_3O_{7-y}$ system has been improved. In more detail, according to weak coupling theory, the existence of oxygen in the material production process and optimum Mn impurity in the crystal matrix has been noted to promote more nest formation near the four points of the antiferromagnetic Brillouin zone with spin waves, leading the expansion of superconducting energy gap (related to the Ginzburg–Landau order parameter) due to the reduction of the thermal fluctuations in main matrix [103]. Namely, the wave systems of spin-density in the $YBa_2Cu_3O_{7-y}$ superconductors have strongly been supported to form the super-electrons and cooper-pairs. However, the excess manganese impurity has damaged seriously the quantum mechanical, basic physical and thermodynamics fields related the T_c^{onset} and T_c^{offset} values as a result of the complete reversal of the quantum mechanical phenomena. One can see also the variation of ΔT_c values of pure and manganese added $YBa_2Cu_3O_{7-y}$ superconductors in Table 4.2. It has been apparent from the table that the pure sample has had the moderate value of 1.466 K whereas the minimum value of ΔT_c has been recorded to be about 0.963 K for the OMn-3 superconducting sample. However, we should declare that the OMn-4 superconducting sample with the highest transition temperatures have exhibited the relatively larger ΔT_c value such as 2.184 K due to the homogeneity problems in the oxidation states and the nesting formation at the vicinity of antiferromagnetic Brillouin zone. It is obvious that the OMn-4 superconductor needs saturation of antiferromagnetic Cu–O chains in the *b*-axis with more oxygen. This problem might be solved by means of more annealing time under oxygen ambient conditions. All in all, exactly as anticipated that the idea of manganese impurity addition (provided that the addition amount is optimal) in the $YBa_2Cu_3O_{7-y}$ system has seemed to be successful to improve the basic electrical conductivity and superconducting features for potential application fields.

4.1.2 Alteration of Charge Carrier Concentrations in Valence Bands of Perovskite-Based $YBa_2Cu_3O_{7-y}$ Cuprate Superconductors with Manganese Impurity and Oxygen Ambient

The last part related to the temperature-dependent resistivity curves is interested in the evolution of mobile charge carriers in the strongly covalently bonded Cu-O_2 layers of $YBa_2Cu_3O_{7-y}$ system. As well kwon, charge carrier number is adjusted by stoichiometry of chemical contents, oxygen excess, variation of decrease/increase in the vacancies in the unit cell, and charge transfer mechanism (reduction/oxidationstates) in the skeleton layers. Hence, the hole concentration level can be enhanced by cation-vacancy, anion/cation-substitution, metal addition, and oxygen-excess. In the current study, we have added the manganese ions in the $YBa_2Cu_3O_{7-y}$ main matrix to increase the charge carrier concentrations in valence bands and stabilize the structure. Even, the enhancement in the transition temperatures has shown the increase in the carrier concentrations. The improvement in the carrier densities has stemmed from the fact that there is a high probability of replacement of the manganese ions for the yttrium ions due to the close of 4p-block bands of host yttrium atoms to the short-range ordered antiferromagnetic Cu-O chains. Thus, the manganese addition in the optimum stoichiometry of chemical content compositions has resulted in the induction of carrier concentrations in the oxygen sites, and the superconducting properties have developed.

The change of the charge carrier concentrations in the σ antibonding in-plane Cu-O chains can also be explained by using the band picture depending on effective one-electron Hamiltonians in the electronic structures [106] which includes the delocalized nature of conduction electrons meaning the change of copper oxidation state. In oxygen deficit perovskite-based cuprate type-II materials, the in-plane $x^2 - y^2$ band for the antiferromagnetic Cu–O chains possesses rather greater energy in comparison with other d-block bands. In the bands the d_{x2-y2} orbital symmetry for the copper gets interaction with the orbitals of the oxygen by making the σ antibonding in-plane Cu-O bonds [107,108], and thus the orbital hybridization is carried out between copper ‘d’ and oxygen ‘p’ orbitals. That is exactly why the addition of foreign impurity affects electronically the orbital hybridization (overlapping of Cu-3d and O-2p wave functions) as a result of the increase/decrease in the hole trap energy. In the present work, the presence of oxygen and optimum manganese impurity has considerably strengthened the interaction in the σ antibonding in-plane Cu-O bonds rather than that in the out-of-plane Cu-O bonds in the weakly coupled Cu-O_2 layers[109]. Correspondingly, the manganese ions have contributed to the positive to the charge carrier concentration number due to the decrease in the hole trap energy distribution in the $YBa_2Cu_3O_{7-y}$ main matrix [110]. At the same time, the bipolaron formation mechanism declares that the increase in the charge carrier concentrations with the optimum manganese impurity addition has caused the localization of the polarons or bipolaronsin the polarizable lattices to form the newpolaronic states (super-electrons and cooper-pairs) in the clusters of microdomains, improving considerably the superconductivity phenomenon.

Finally, the change in the superconducting behavior can also be clarified in detail by the pairing mechanism. That is, the pair wave function ($\Psi= \Psi_0 e^{-i\varphi}$) includes two important participants. The first one is the amplitude part (Ψ_0) related to the number of super-electrons while the second one is phase coherence part ($e^{-i\varphi}$) corresponded to the supercurrent [111, 112]. According to the electrical curves given in Figure 4.1 and Figure 4.2, it is clear that the phase coherence part has not been affected (due to the completely disappearance of superconducting phenomenon for the $YBa_2Cu_3O_{7-y}$ superconductors). On the contrary, the presence of oxygen and optimum Mn_2O_3 impurity in the main matrix has positively affected only Ψ_0 part of pair wave function depending on the increase in the number of thermodynamically activated super-electrons [113,114].

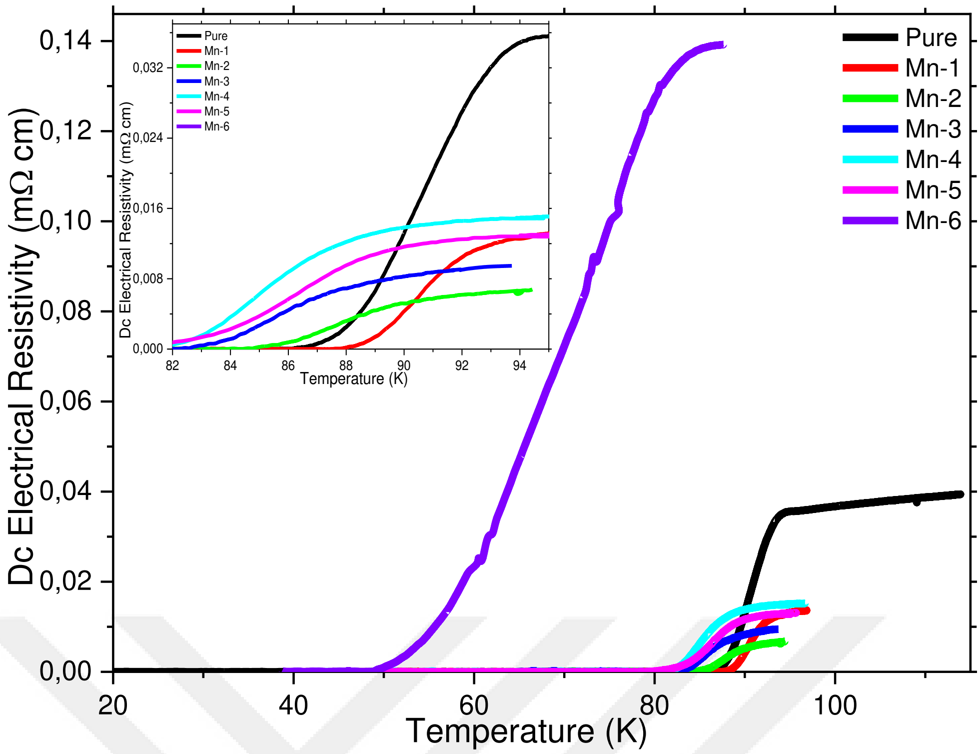

Figure 4.1: Pure and Mn added bulk $YBa_2Cu_3O_{7-y}$ superconductors prepared at without the oxygen ambient condition.

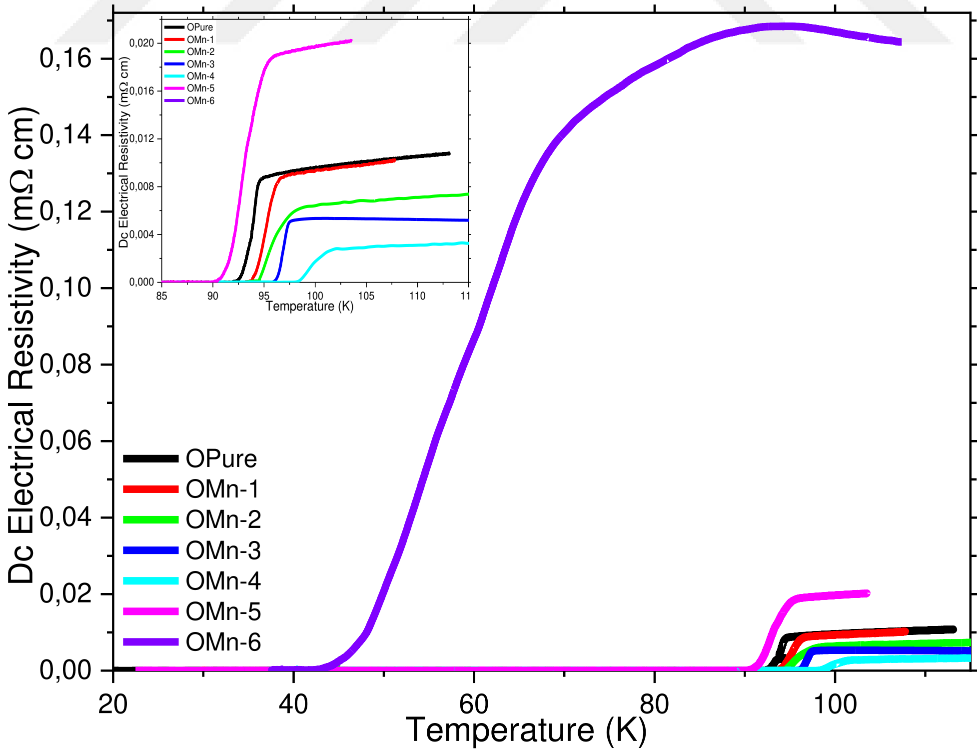

Figure 4.2: Pure and Mn added $YBa_2Cu_3O_{7-y}$superconductors produced under the oxygen ambient condition.

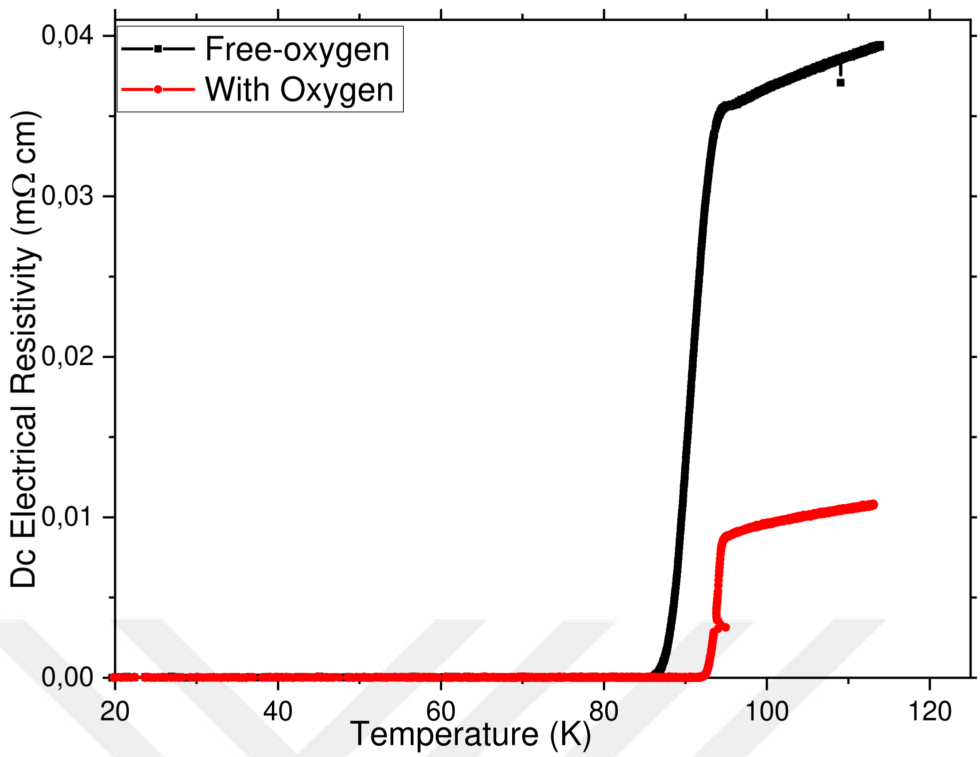

Figure 4.3: Two pure samples prepared at oxygen and oxygen-free annealing ambient.

4.2 Changes in Transport Critical Current Density Searches

Three main properties including the high current carrying ability, large critical transition temperature, and high magnetic field carrying capacity are effective in deciding the use of the material in the potential application fields of industrial power systems and energy-related sectors. Thus, the critical current density (J_c) is important supporting evidence to confirm the effect of oxygen ambient and Mn_2O_3 impurity on the fundamental characteristics of $YBa_2Cu_3O_{7-y}$ superconductors. However, the non-recoverable microscopic structural problems, anisotropic nature (various crystalline directions of superconducting grains), granular, and especially layered structure restrict the application areas of oxygen deficit perovskite-based cuprate Type-II materials. Hence, the applied magnetic field and current accelerate seriously the motions of thermal flux on vortices (fluxons) in 2D pancake vortices due to the weak performance features depending on the strength and ability of elasticity, vortex lattice period, and flux pinning nucleation of $YBa_2Cu_3O_{7-y}$ superconductor. With the thermal motions, the 2D pancake vortices overcome their pinning barriers and jump to those in the near neighboring states including relatively higher energy barriers. This effect is known to be the cooper pair-breaking mechanism [115, 116] where thermal fluxons appear to be of discrete pancake-like (recoupling linelike) nature due to the decoupling of adjacent multilayers. Shortly, the movement of 2D vortices result in the conversion of electrical energy to the heat energy as a consequence of the appearance of ohmic resistance, energy losses and energy dissipation in the superconductors [117]. In this work, we have endeavored to delay the beginning of energy dissipation in the $YBa_2Cu_3O_{7-y}$ main matrix with the aid of manganese impurity addition and oxygen annealing ambient by enhancing the artificial flux pinning centers, interaction quality between grains, pinning ability and strength quality of 2D coupled vortices. For this aim, we have thoroughly made the standard transport critical current density tests at the liquid nitrogen of 77 K without any applied magnetic field. We have preferred the transport experiments instead of the magnetic measurements due to more reliable results [118]. In other words, in the magnetic measurements the experimental signals are obtained over the entire sample and thus the microcrystal coalescencemisorientations, granular structure, grain alignment distributions and orientations, internal defects, porosity, microvoids, intragrain and inter-grain boundary couplings, and non-recoverable microscopic problems are totally ignored [119, 120]. Namely, the researchers obtain very higher critical current density values than expected, and the magnetic measurement results obtained can be misleading the researchers for the use of the material in the potential application fields of industrial power systems and energy-related sectors. One can see all the self-field J_c parameters for the pure and Mn-added perovskite-based $YBa_2Cu_3O_{7-y}$ cuprate superconductors produced under oxygen ambient conditions and different Mn_2O_3 impurity addition amount in Table 4.3 and Table 4.4. It is found from the tables that the J_c values have been observed to sensitively depend on the oxygen ambient and Mn_2O_3 impurity. Numerically, similar to the change in the electrical resistivity and superconducting features, the oxygen ambient condition has ben noted to affect positively the values of J_c parameter. In this context, the pure $YBa_2Cu_3O_{7-y}$ superconductor fabricated at oxygen ambient conditions has exhibited the J_c value of about 62 A/cm^2, the other pure sample has possessed the J_c value of about 57 A/cm^2. Additionally, the increase in the Mn_2O_3 impurity addition has damaged seriously the number of flux pinning centers in the Mn-added $YBa_2Cu_3O_{7-y}$ superconductors prepared without the oxygen ambient conditions. Thus, we have focused on the J_c values of Mn-added $YBa_2Cu_3O_{7-y}$superconductors produced under the oxygen ambient conditions. On this basis, the J_c values have been observed to augment remarkably with the Mn_2O_3 impurity addition amount up to x=0.07 beyond which the parameters have been obtained to decrease considerably due to the improvement in the artificial flux pinning centers, interaction quality between grains, pinning ability and strength quality of 2D coupled vortices. In this respect, the OMn-4 sample has possessed the highest J_c value of 98 A/cm^2. As for the maximum manganese added sample, the J_c value has been observed to diminish towards the value of 38 A/cm^2. The experimental findings have shown that the presence of optimum manganese impurity addition in the $YBa_2Cu_3O_{7-y}$superconductor has served as the artificial flux pinning nucleation sites to retard the beginning of energy dissipation depending on the thermally activated 2D pancake vortices [121-124]. Namely, the manganese impurity highly dispersing throughout the intra grain and inter-grain boundary couplings has been noted to bind tightly the adjacent layers [125–127]. With the enhancement in the artificial flux pinning nucleation sites, the bulk OMn-4 superconductor has exhibited the most resistance to the applied magnetic field and current strengths [128]. Besides, the suppression in the microscopic structural problems has been reazlied to be the other positive effect on the increase of J_c value. Conversely, the excess manganese ions have been found to significantly damage the flux pinning centers and related structural problems in the $YBa_2Cu_3O_{7-y}$ superconductor. Additionally, the rapid decrement in the J_c value may be resulted from the aggregation of excess impurity ions over the grain boundary sites.

Table 4. 3: Experimental data Oxygen free ambient.

Samples	*a (Å)*	*b (Å)*	*c (Å)*	*t (nm)*	*y (c)*	*δ = b -a/b +a (10^{-3})*	*Strain (10^{-3})*	*Dislocation densities* **(10^{-3} nm^2)**	*Ratio of Dislocation densities (relative value %)*	*Ratio of Dislocation densities (relative to optimum material value %)*	***J_c (A.cm^{-2})***	***J_c (A.cm^{-2})***
Pure	3,762	3,788	11,705	19,15	6,833	3,444	78,72067	16,39051	11,17328	222,4283	57	57
Mn-1	3,744	3,779	11,712	20,24	6,787	4,652	74,48127	14,74321	0	190,0232	64	64
Mn-2	3,772	3,795	11,701	18,46	6,860	3,040	81,6631	17,59194	19,32232	246,0624	53	53
Mn-3	3,779	3,801	11,698	18,26	6,880	2,902	82,55755	17,94611	21,72458	253,0295	51	51
Mn-4	3,786	3,808	11,692	17,32	6,920	2,897	87,03815	19,91005	35,04556	291,6634	48	48
Mn-5	3,792	3,811	11,689	16,76	6,940	2,499	89,94635	21,22914	43,99266	317,6121	45	45
Mn-6	3,802	3,82	11,686	15,65	6,960	2,362	96,32593	24,28332	64,7085	377,6928	42	42

Table 4. 4: Experimental data with oxygen ambient.

Samples	*a (Å)*	*b (Å)*	*c (Å)*	*t (nm)*	*y (c)*	*δ = b -a/b +a (10^{-3})*	*Strain (10^{-3})*	*Dislocation densities* (10^{-3} nm^2)	*Ratio of Dislocation densities (relativistic value %)*	J_c *($A.cm^{-2}$)*
Pure	3,818	3,855	11,708	20,43	6,813	4,822	73,78859	14,1898	179,1367	62
OMn-1	3,81	3,854	11,709	21,65	6,807	5,741	69,63052	12,66217	149,0857	67
OMn-2	3,808	3,853	11,711	21,69	6,793	5,874	69,50211	12,62213	148,2981	76
OMn-3	3,804	3,849	11,718	30,97	6,747	5,880	48,67616	6,197634	21,91765	89
OMn-4	3,792	3,841	11,723	34,25	6,714	6,419	44,01462	5,083459	-------	98
OMn-5	3,827	3,863	11,694	19,51	6,907	4,681	77,26811	15,52301	205,3631	57
OMn-6	3,838	3,871	11,691	19,13	6,927	4,281	78,80297	16,09956	216,7048	38

4.3 SEM Analysis

In this part of paper, scanning electron microscopy (SEM) investigations have been performed not only to observe the evolution of surface morphology appearance and crystal structure quality of $YBa_2Cu_3O_{7-y}$superconductor with the oxygen annealing ambient condition and different manganese impurity addition level but also to support the experimental findings obtained in other parts in detail. SEM photomicrographs belonging to the pure and Mn-added $YBa_2Cu_3O_{7-y}$ superconductors have been taken at accelerator voltage of 20 kV in the SEI (secondary electron image) mode with 5000X magnification. We have provided the pure superconductors produced with and without oxygen annealing ambient condition in Figure 4.4-4.5. It is obvious from the pictures that the presence of oxygen during the annealing process has been noticed to develop the appearance of surface morphology and crystallinity quality for the $YBa_2Cu_3O_{7-y}$ superconductors. In this regard, we have given all the photomicrographs of Mn-added $YBa_2Cu_3O_{7-y}$ superconductors prepared at the oxygen annealing ambient conditions in Figure 4.6-4.11. It is apparent from the images that the enhancement in the manganese impurity has been found to change dramatically the grain alignment distributions and orientations, grain boundary regions, interaction quality between grains, and basic structural morphology appearances (uniform surface view, impurity residues, microscopic structural problems, internal defects, porosity, particle growth distribution, micro voids, microcrystal coalescence orientations, and partial melting regions). In this context, the surface morphology appearance and crystal structure quality have been recorded to develop dramatically with increasing the manganese impurity addition level up to x=0.07 value where the OMn-4 superconductor has possessed the most uniform, highest crystallinity quality, smoothest, densest surface views, largest particle growth size (well linked) distributions, largest connection between particles, best connectivity between the grains and grain alignment orientations. Besides, the OMn-4 superconductor with the lowest porous structure has been recorded to show the strong interatomic bonding forces, inter planar bonds and couplings between adjacent layers as seen in Figure 4.9. Conversely, beyond the impurity addition level of x=0.07, the surface morphology appearance and crystal structure quality of the Mn-added $YBa_2Cu_3O_{7-y}$ superconductor have been observed to diminish dramatically, and in fact the features have been noted to reach the worst states for the OMn-6 superconductor. This is because the excess manganese impurity addition has triggered the formation of impurity phases and microscopic structural problems.

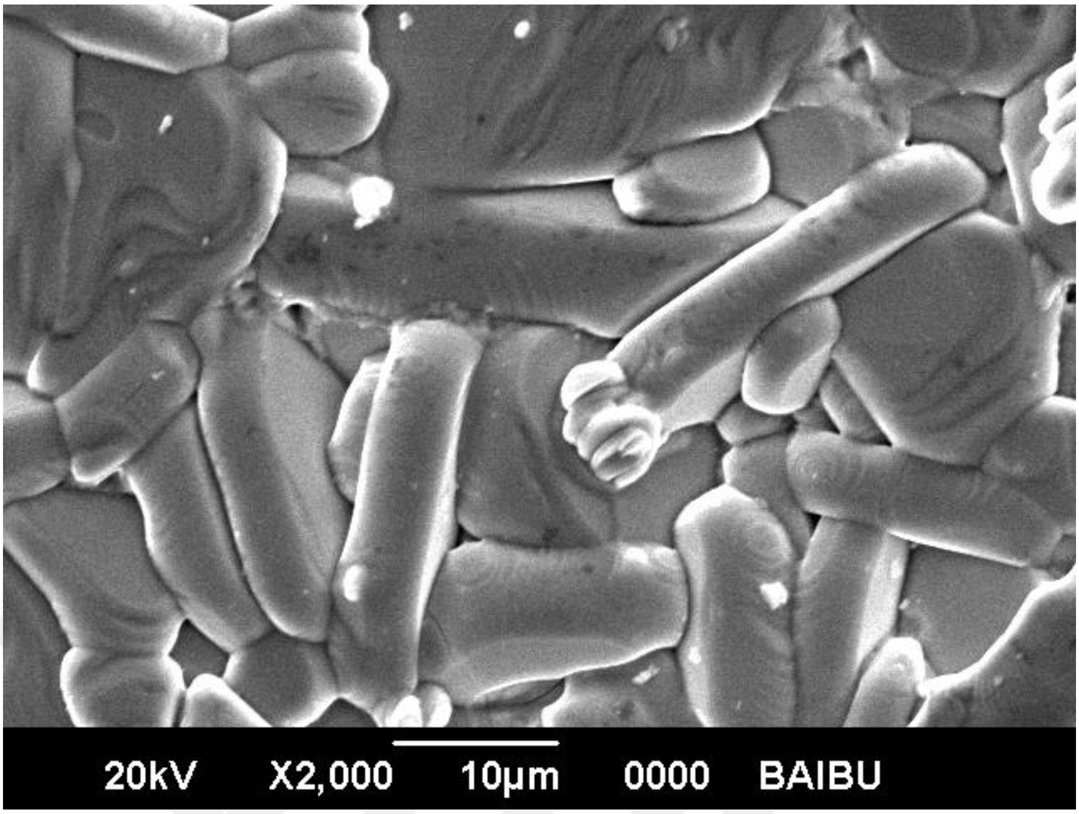

Figure 4.4: The pure superconductors produced with oxygen annealing ambient condition.

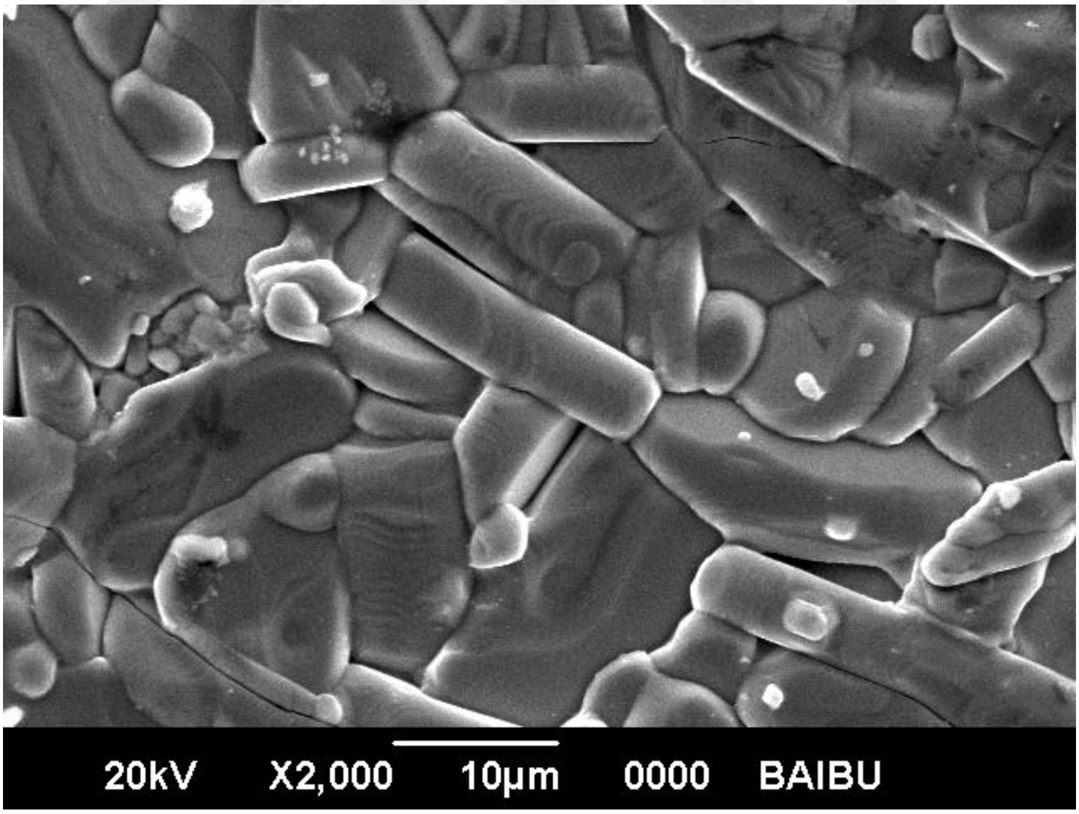

Figure 4.5: The pure superconductors produced without oxygen annealing ambient condition.

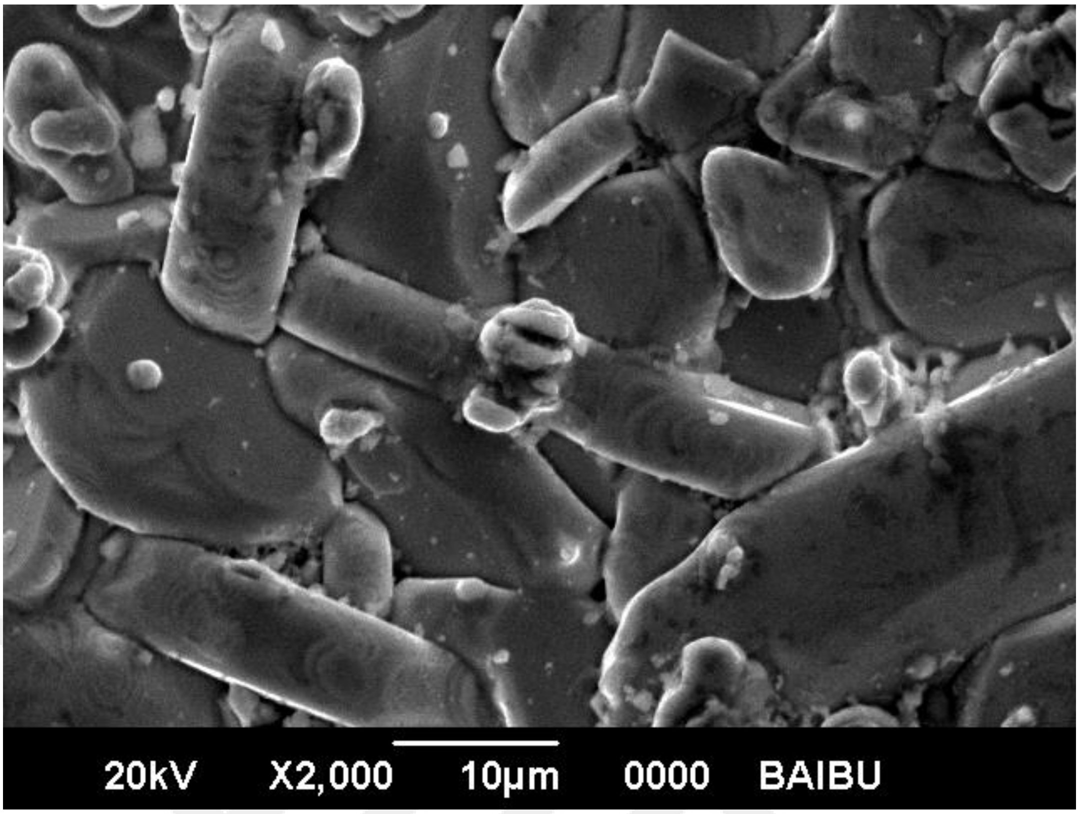

Figure 4.6: Sem photographics of Mn (0.01) added YBCO superconductors prepared at the Oxygen ambient conditions.

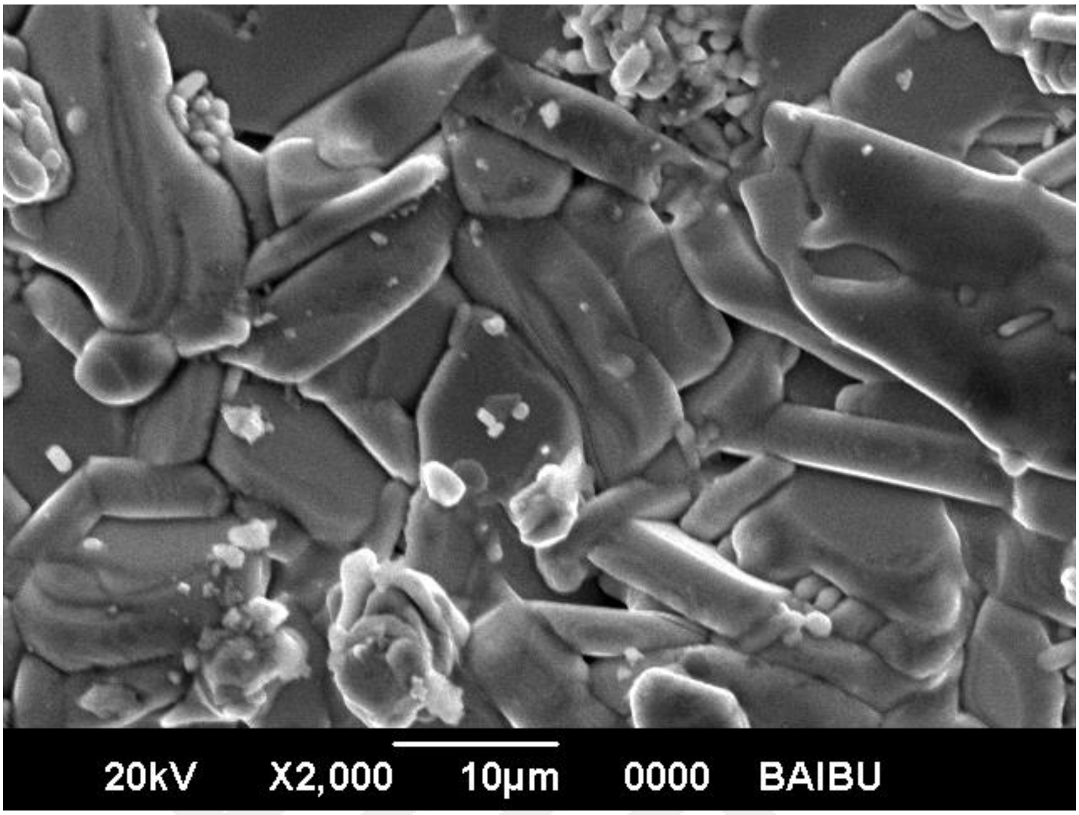

Figure 4.7: Sem photographics of Mn (0.03) added YBCO superconductors prepared at the Oxygen ambient conditions.

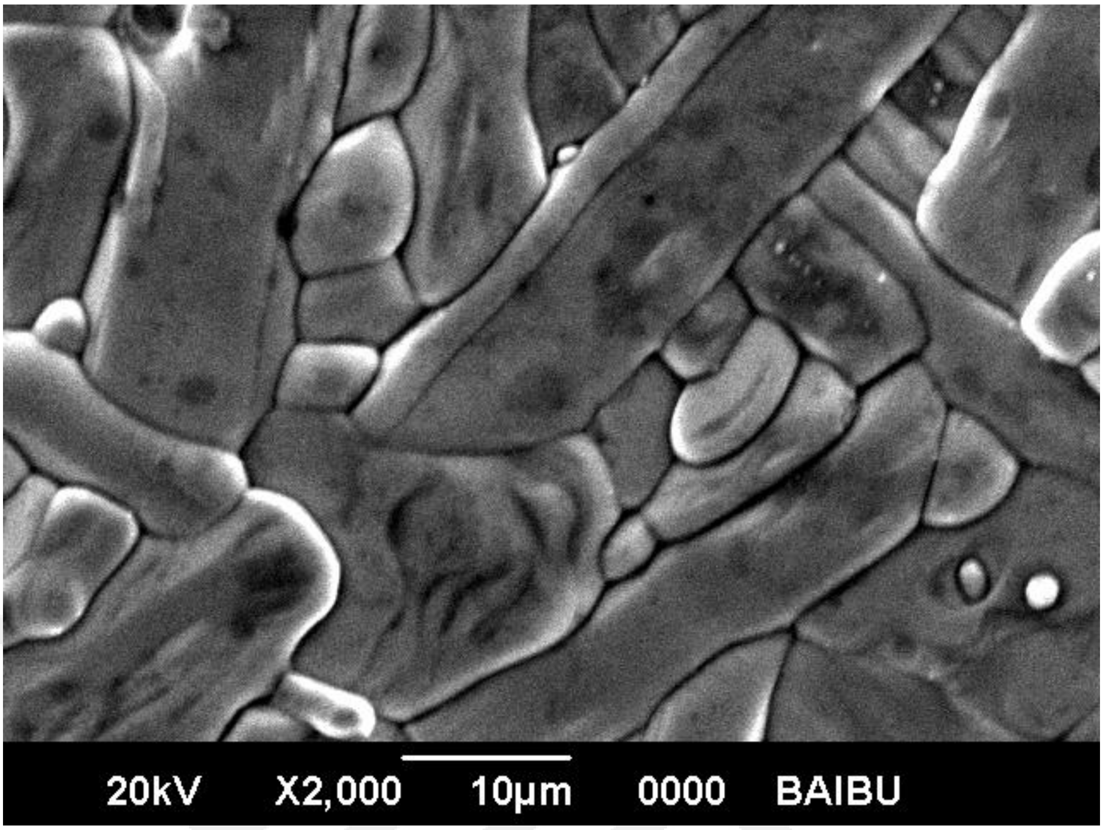

Figure 4.8: Sem photographics of Mn (0.05) added YBCO superconductors prepared at the Oxygen ambient conditions.

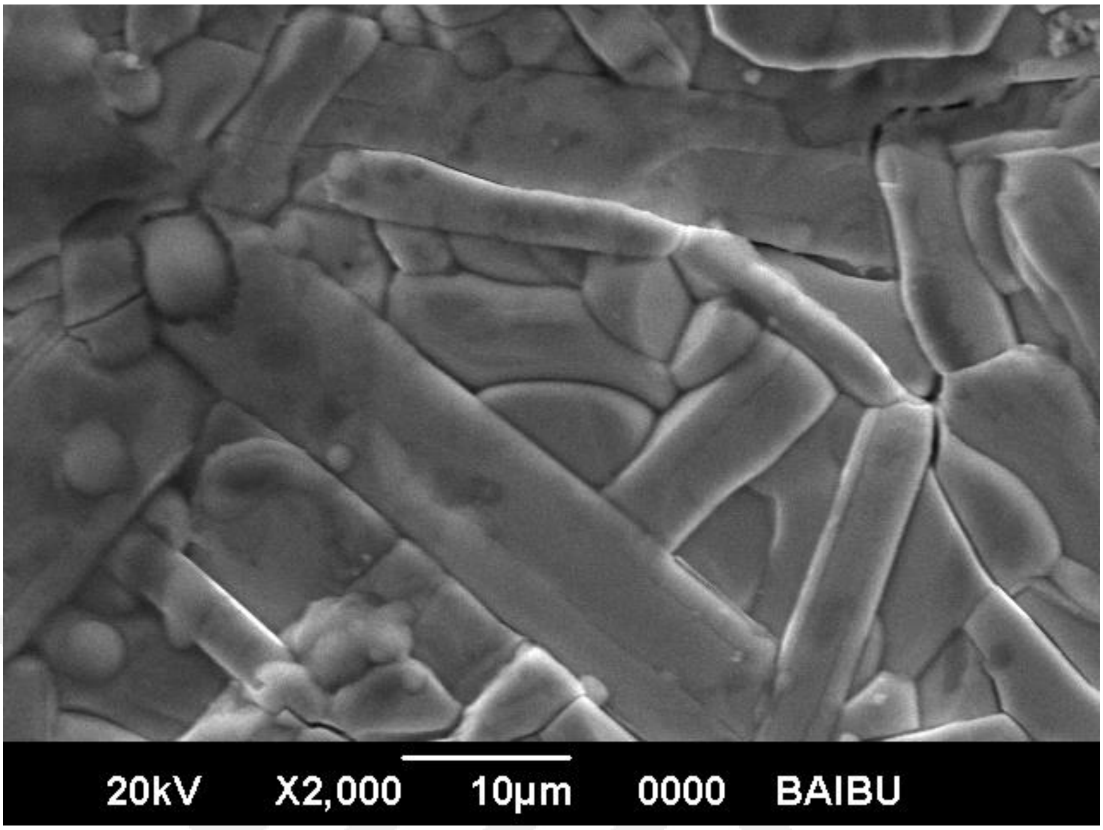

Figure 4.9: Sem photographics of Mn (0.07) added YBCO superconductors prepared at the Oxygen ambient conditions.

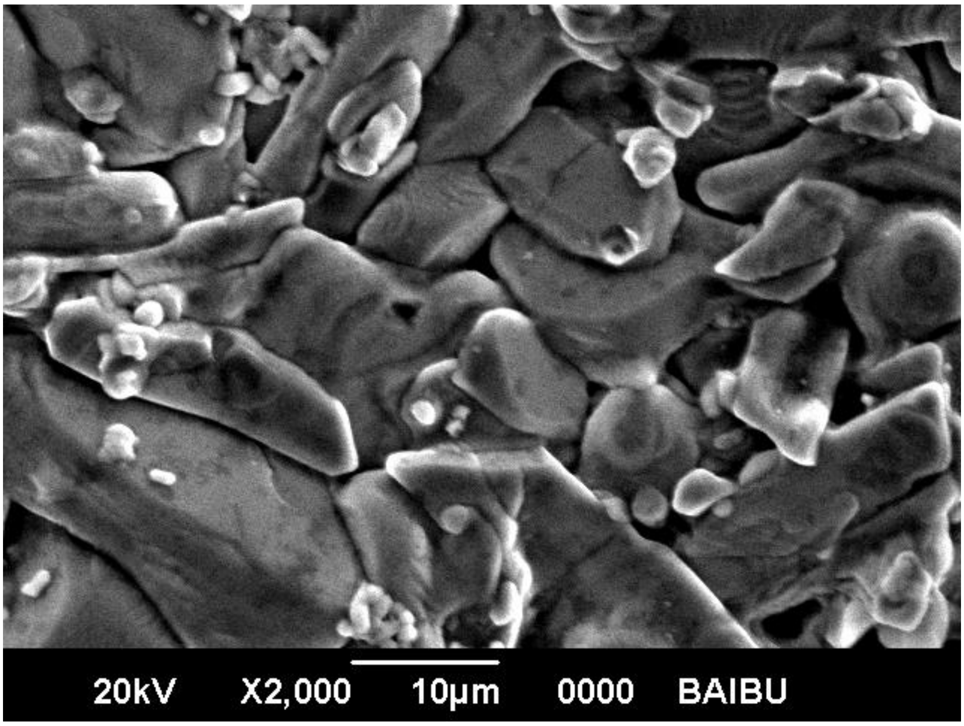

Figure 4.10: Sem photographics of Mn (0.10) added YBCO superconductors prepared at the Oxygen ambient conditions.

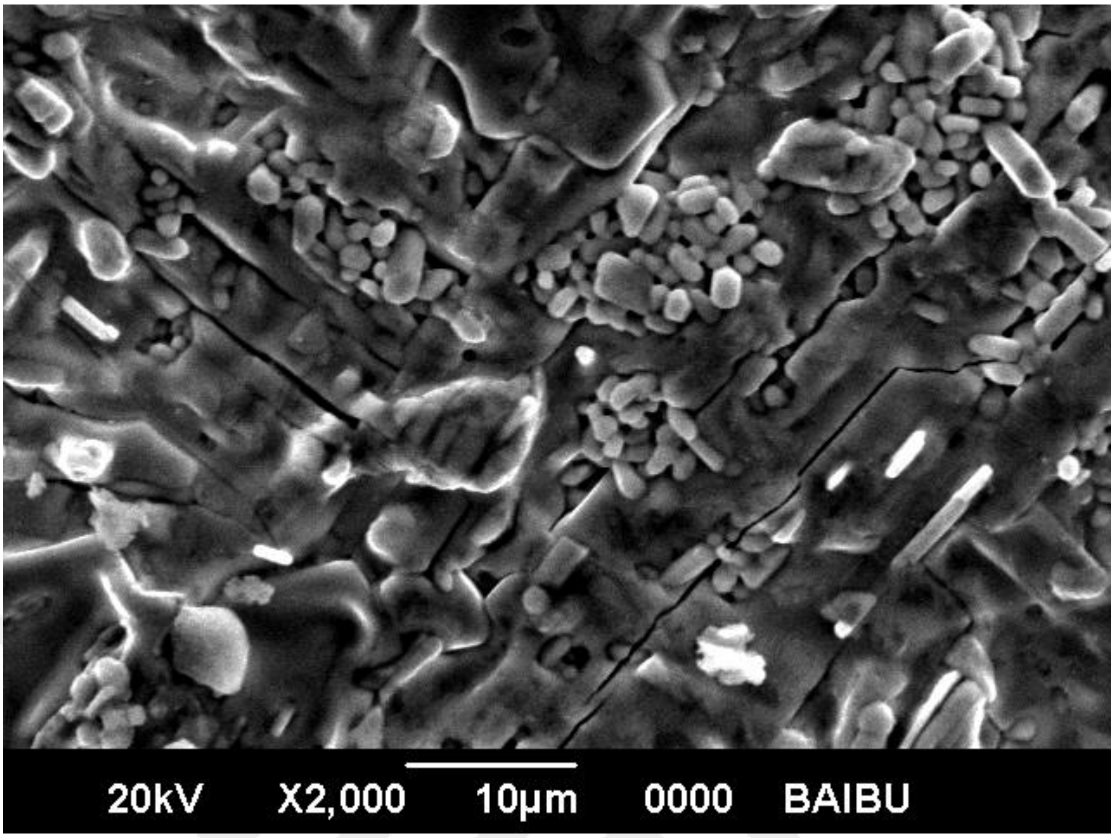

Figure 4.11: Sem photographics of Mn (0.30) added YBCO superconductors prepared at the Oxygen ambient conditions.

4.4 XRD Diffractogramsfor $YBa_2Cu_3O_{7-y}Mn_x$ Ceramic Compounds Prepared at Different Annealing Ambient Conditions

The evolutions of the fundamental crystal structural parameters such as crystallization system, lattice cell constants, distributions of grain alignments, crystallinity quality, phase volume fractions, oxygen ordering degree, orthorhombicity, structural O–T transition, average crystallite size, oxygen concentrations in unit cell, lattice strains, and dislocation densities of the $YBa_2Cu_3O_{7-y}$ superconductors with the oxygen annealing ambient condition and different Mn_2O_3 impurity addition amounts have extensively been searched by the characteristic peak reflections in the XRD diffractograms. One can see the well-defined XRD patterns preformed at 2θ angles varying from 3° to 60° in Figure 4.12 (pure and Mn added bulk $YBa_2Cu_3O_{7-y}$superconductors prepared at without the oxygen ambient condition) and Figure 4.13 (pure and Mn added $YBa_2Cu_3O_{7-y}$ superconductors produced under the oxygen ambient condition). According to the XRD graphics given, every sample (whether prepared at oxygen annealing ambient or not) has been recorded to exhibit the typical polycrystalline behavior within the crystalline solid property with long-range atomic arrangement and 3D network periodicity spread in all directions in a highly ordered microscopic structure. Additionally, the presence of oxygen ambient and Mn_2O_3 impurity in the crystal system has caused the disappearances/new occurrences of characteristic diffraction peaks, broadening of full width at half maximum (FWHM), shifts of the peaks to the low/high 2θ angles, and increase/decrease in the diffraction intensities due to the re-modification of skeleton layers. The re-ordering of geometrical structures has verified that the Mn_2O_3 impurity has successfully been entered in the $YBa_2Cu_3O_{7-y}$ superconductors. The diffraction peaks have been marked by Miller indices of *hkl* in Figure 4.12, Figure 4.13, and Figure 4.14. According to the figures, it is obvious that all the materials have exhibited mainly the characteristic $YBa_2Cu_3O_{7-y}$ (Y-123) superconducting phase in their crystal structures within the different diffraction intensities. In Figure 4.14 we have depicted the typical XRD graphics for the pure $YBa_2Cu_3O_{7-y}$ superconductors produced under the oxygen and oxygen-free annealing ambient conditions. It is apparent from the XRD diffractograms that the existence of oxygen ambient has improved the crystal structure of pure $YBa_2Cu_3O_{7-y}$

superconductor. Besides, the main characteristic diffraction peak of *003* has appeared immediately with the oxygen. Thus, the $YBa_2Cu_3O_{7-y}$ characteristic phase in the crystal structure has been noted to be supported by the oxygen ambient. Also, the change in the crystallinity quality with the Mn_2O_3 impurity addition amount of $YBa_2Cu_3O_{7-y}$ crystal structure has been provided in Figure 4.12, and Figure 4.13, respectively. The experimental findings have shown that both the presence of oxygen and optimum Mn_2O_3 impurity amount in the crystal system have seriously favored the characteristic $YBa_2Cu_3O_{7-y}$ phase. In this content, we have discussed only the experimental test results (Figure 4.13) for the samples produced at the oxygen ambient conditions. It has been seen that all the $YBa_2Cu_3O_{7-y}Mn_x$ superconductors have been found to crystallize in the orthorhombic crystal structure with $P_{4/mmm}$ space group in a few distortions. With the increase in the Mn_2O_3 impurity amount up to the level of x=0.07, the orthorhombic crystal system has been noted to develop systematically. However, the excess manganese ions have caused the beginning of the pseudotetragonalcrystal system, and in fact the OMn-5 superconductor has shown the dominant character of pseudotetragonal crystal system. At the same time, the shift of diffraction peaks allows us to find the influence of oxygen annealing ambient and manganese impurity addition on *a*, *b*, and *c* lattice cell constants to study the phase transition from orthorhombic to tetragonal (OT transition) crystal structure. It depends on the difference in the oxygen content of the crystalline Cu-O chains and Cu-O layers. One can see the lattice cell parameters in Table 4.3 and Table 4.4. It is found that all the calculated parameters have been obtained to agree with the literature data. Numerically, the $YBa_2Cu_3O_{7-y}$ superconductors prepared at the oxygen annealing ambient have exhibited higher *c* lattice cell constant parameters. In this respect, the OMn-4 sample has had the maximum *c*-axis length of 11.723 Å whereas the minimum value of 11.691 Å has been found for the OMn-6 sample. Among the $YBa_2Cu_3O_{7-y}$ superconductors produced without the oxygen annealing ambient conditions, the bulk Mn-6 superconductor has had the smallest *c*-axis length of 11.686 Å. As for the *a* and *b*-axis lengths, the OMn-4 sample has had the smallest values (Table 4.4). Additionally, we have been interested in the effect of oxygen annealing ambient and manganese oxide impurity addition amount on the oxygen concentration levels in the unit cell with the aid of differentiation in the lattice cell constants. This is because for the orthorhombic crystal system of $YBa_2Cu_3O_{7-y}$superconductor the oxygen-deficient plays a serious role on the transition temperature values. As well known that when the stoichiometric ratio related to the oxygen content of $YBa_2Cu_3O_{7-y}$ system is nearly 0.15, the structure crystallizes in the orthorhombic P_{mmm} symmetry and thus the material has the maximum transition temperature value. Nevertheless, when the letter of y in the system reaches the value of 0.6, the main orthorhombic phase transits to the tetragonal symmetry [129]. Thus, the superconductivity vanishes slowly and slowly. The following relation gives us to determine the change in the oxygen concentration levels in the unit cell for the Mn added $YBa_2Cu_3O_{7-y}$ superconductor [130]:

$$y = 7 - \frac{c - 11.68}{0.1501} \qquad (1)$$

According to the relation, the *c*-axis length is in charge of the oxygen concentration levels in the unit cell. Even, it is received that the formation of electron-electron and electron-phonon interactions, and bipolarons in the polarizable lattices is due to the presence of *c*-axis phonons in the system. The calculated parameters have numerically been depicted in Table 4.3 and Table 4.4. It is seen from the tables that all the bulk $YBa_2Cu_3O_{7-y}Mn_x$ superconductors have exhibited close values to each other. However, under the existence of oxygen in the annealing ambient conditions the $YBa_2Cu_3O_{7-y}Mn_x$ samples has presented relatively lower y values (results closer to the optimum oxygen concentration levels). In this respect, we have discussed only the variation in the oxygen concentration levels in the unit cell with the manganese impurity addition amount. Table 4.3 has indicated that as the manganese impurity addition amount has increased in the $YBa_2Cu_3O_{7-y}$ system up to x=0.07, the value of y parameter has been noted to reduce systematically. On this basis, the MnO-4 sample has shown the minimum y value of 6.714. After x=0.07, the oxygen concentration levels in the unit cell have been found to increase immediately. For the maximum impurity addition level of x=0.30, the value of y parameter has been obtained to be about 6.927. The dramatic changes with the manganese impurity addition have been due to the decrement in the *c*-axis length. At the same time, the effect of annealing ambient conditions and manganese impurity addition level on the orthorhombic distortion (or known as the oxygen ordering degree) in the covalently bonded Cu–O ribbons by using the formula of (b-a)/(b+a) [130, 131]. According to the equation, the size of the difference between the lengths of *b*- and *a*-axes for the $YBa_2Cu_3O_{7-y}$ superconductors determines the orthorhombic distortion degree [132]. One can encounter the computations for the parameters of oxygen ordering degree in Table 4.4 (including the data for the $YBa_2Cu_3O_{7-y}Mn_x$ superconductors produced at the oxygen annealing ambient) and Table 4.3 (presenting the results for the $YBa_2Cu_3O_{7-y}Mn_x$ superconductors produced without the oxygen ambient). It is seen from the table that the former materials have had much higher orthorhombic distortion values than those of the latter samples. This is because the presence of oxygen ambient has been noted to encourage the formation of orthorhombic crystal structure in the $YBa_2Cu_3O_{7-y}$ materials. Likewise, rather larger crystalline structures have been obtained in the case of the oxygen annealing ambient, having already been favored by the SEM investigations. Correspondingly, we have sensitively focused on the change of the oxygen ordering degrees (δ) for only the bulk $YBa_2Cu_3O_{7-y}Mn_x$ superconductors produced at the oxygen annealing ambient. In this respect, the pure $YBa_2Cu_3O_{7-y}$ material has observed the moderate δ parameter of $4.822x10^{-3}$. With the increase in the Mn_2O_3 impurity amount in the crystal system up to x=0.07 the values of δ parameter have been obtained to increase systematically. In this respect, the OMn-4 sample has obtained the highest orthorhombic distortion degree of $6.419x10^{-3}$. Beyond the optimum manganese impurity addition amount of x=0.07, the orthorhombic distortion parameter has been observed to decrease dramatically, and the minimum value of $4.281x10^{-3}$ has been recorded for the highest Mn-added $YBa_2Cu_3O_{7-y}$ sample among all the superconductors produced at the oxygen annealing ambient conditions. Shortly, the bulk OMn-4 superconductor has been determined to have the complete oxygen ordering meaning the empty O-5 sites and fully filled O-1 sites due to the improved crystallization system, couplings between adjacent layers, and connectivity between the Mn impurity and host ions in the main matrix. At the same time, the broadening structure of XRD patterns has enabled us to define the role of oxygen and Mn_2O_3 impurity addition amount on the differentiation of average crystallite sizes of $YBa_2Cu_3O_{7-y}Mn_x$ superconductors. For the calculation of the grain sizes, we have used Scherrer–Warren approach related to the FWHM parameters [133, 134]. Namely,

$$t = 0.941\lambda \big/ B\cos\theta_B \qquad (2)$$

in the equation, when t shows the crystallite size, λ is related to the wavelength of incident X-rays, and the abbreviation of Θ_B displays the Bragg angle for the diffracted beams. In the relation, B indicates the value of FWHM parameter for the Bragg diffraction peak. We have depicted the deduced average crystallite size values in Table 4.4 (including the data for the $YBa_2Cu_3O_{7-y}Mn_x$ superconductors produced at the oxygen annealing ambient) and Table 4.3 (presenting the results for the $YBa_2Cu_3O_{7-y}Mn_x$ superconductors produced without the oxygen ambient). When comparing the gran size parameters for the pure samples, it has been recorded that the presence of oxygen ambient in the annealing process has made the crystallite size increase. Thus, we have given the detail for the $YBa_2Cu_3O_{7-y}Mn_x$ superconductors prepared at the oxygen annealing ambient. Table 4.3 has demonstrated that the average crystallite size value has been found to increase regularly with the increase in the manganese impurity addition amount up to x=0.07. On this basis, the OMn-4 sample has had the maximum crystallite size of 34.25 nm. On the other hand, the excess manganese impurity has led to the decrement in the crystallite size value, and in the case of x=0.30 the t value has been recorded to be about 19.13 nm that has been the smallest value among the superconductors prepared at the oxygen annealing ambient. Additionally, of all the $YBa_2Cu_3O_{7-y}Mn_x$ samples the minimum value grain size value has been noted to be about 11.180 nm for the Mn-6 sample (Table 4.4). The computations have displayed that the oxygen annealing ambient and optimum Mn ions in the crystal structure have been observed to develop the crystallization system, couplings between adjacent layers (based on the diminish in the microscopic structural problems), and connectivity between the Mn impurity and host ions in the main matrix, having already been supported by the SEM investigations. Also, the diffraction peaks in the XRD diffractograms have enabled us to find the influence of both the oxygen and manganese impurity addition amount on the inhomogeneous distributions of lattice strains depending on the grain orientations, grain growth distribution, lattice parameters, and microscopic structural problems in the main crystal lattice. The lattice strains (calculated with respect to Eq. 3) for the bulk $YBa_2Cu_3O_{7-y}Mn_x$ samples determined have been depicted in Table 4.3 and Table 4.4.

$$\varepsilon = Bcos(\theta/4) \quad (3)$$

Here B indicates the FWHM value for the Bragg diffraction peak, θ represents the angle belonging to the diffraction peak, and ε shows the strain. It is obvious that the presence of oxygen ambient during the annealing conditions and optimum Mn_2O_3 impurity addition in the crystal structure has been found to degrade gradually the lattice strains in the main matrix. In this respect, the pure sample has exhibited the strain value of 73.886x10^{-4}. In the case of the optimum manganese impurity addition amount, the OMn-4 superconducting sample has had the minimum strain value of 44.072x10^{-4}. On the other hand, the maximum strain value of 78.907x10^{-4} has been observed for the OMn-6 superconducting sample. The bulk YBa2Cu3O7-yMnx samples prepared without oxygen ambient in the annealing process have presented relatively higher strain values between 14.763x10^{-4} (for the Mn-1 superconductor) and 96.453x10^{-4} (for the OMn-6 superconductor). On this basis, the numerical strain values have displayed that the oxygen and optimum manganese impurity have affected positively the grain orientations, grain growth distribution, lattice parameters, and couplings between adjacent layers in the main crystal lattice. We have also determined the alteration of dislocation densities in the bulk $YBa_2Cu_3O_{7-y}$ crystal system with the oxygen ambient and Mn_2O_3 impurity addition with the aid of the equation of $\delta=15\varepsilon/at$ (here a is the lattice constant parameter, ε shows the strain and is deduced from Eq. 3, and t defines the average grain size values) to show how much pressure is exerted on the crystal structure of YBa2Cu3O_{7-y} superconductor. According to the dislocation density parameters given in Table 4.3 and Table 4.4, the superconductors prepared under the oxygen annealing ambient process have exhibited smaller values of δ parameter as compared to those produced without oxygen ambient. Likewise, the optimum manganese addition level has affected positively the dislocation densities in the main matrix. In this regard, the minimum parameter of 5.090x10^{-4} nm^2 has been obtained for the bulk OMn-4 superconductor. Among the $YBa_2Cu_3O_{7-y}$ superconductors produced at the oxygen annealing ambient conditions, the bulk OMn-6 superconductor has had the largest δ value 16.121x10^{-4} nm^2. As for the other $YBa_2Cu_3O_{7-y}$ superconductors prepared without oxygen annealing ambient conditions, the highest dislocation density parameter of 24.315x10^{-4} nm^2 has been obtained for the Mn-6 superconductor. Moreover, we have determined amongst themselves the relative dislocation density ratios based on the best crystal structure of bulk OMn-4 superconductor for oxygen ambient and Mn-2 sample prepared without oxygen ambient. one can see all the relative dislocation density ratios in Table 4.3 and Table 4.4. The variation of density ratios has been found to be between 21.918% (for the OMn-3 sample) and 216,7048% (for the bulk OMn-6 sample). As for the oxygen free ambient, the maximum dislocation density ratio (with respect to the Mn-2 sample) has been noted to be about 64,7085% for the bulk Mn-6 sample. Thus, the excess manganese impurity has been noticed to damage significantly the basic crystallographic properties of $YBa_2Cu_3O_{7-y}$ crystal structure. Finally, we have depicted the relative differentiation of dislocation density ratios with respect to the best (OMn-4) superconducting sample to point out the importance of oxygen and manganese addition for the production of $YBa_2Cu_3O_{7-y}$ superconductor in Table 4.4. It is obvious that the relative ratio has been found to reach the maximum value of 377,6928 for the Mn-6 superconductor. The dramatic increment has shown why all the fundamental characteristic features have degraded without oxygen ambient. As for the reaction kinetics of nucleation (crystallization) mechanism, the changes in diffraction intensities and the shifts of the characteristic peak reflections in the XRD diffractograms with the oxygen annealing ambient condition and Mn_2O_3 impurity addition amount stem from the alteration of activation energy (known as E_a) for the crystallization depending on the stoichiometry of chemical contents in the composition [135]. Even, the nucleation mechanism is received to play an important role in understanding the electrical and superconducting behavior of a superconductor. The experimental findings related to the XRD, SEM, ρ-T, and I-V tests have demonstrated that the existence of oxygen in the annealing process and optimum manganese impurity has resulted in the considerable degradation in the value of E_a parameter because of the variation in the stoichiometry of chemical contents in the composition (based on the changed electronegativity, valance electron states, electron configurations, cation-vacancy, ionic radius dimensions), couplings between adjacent layers, andinterplanar bonds of Mn ions and host ions along with the main matrix [136, 137]. On the other hand, the oxygen-free annealing ambient and excess manganese impurity have caused the remarkable increase in the activation energy value of the oxygen deficit perovskite-based $YBa_2Cu_3O_{7-y}$ superconductor due to the shift of the crystallization temperature to lower temperature regions. Namely, the crystallization mechanism of different impurity phases (detected in the XRD patterns) has started in the $YBa_2Cu_3O_{7-y}$ matrix instead of the main characteristic superconducting phase. As for the best Mn-added bulk $YBa_2Cu_3O_{7-y}$ (OMn-4) sample, the material preparation conditions mentioned above have led the enhancement in the nucleation temperatures towards higher temperature regions. In the rearrangement procedure to nucleate the different phases, the chemical contents that bind with neighboring ions in the main composition are placed in the lattice state of the primary crystals [138]. As for the nucleation stability of pure and Mn added bulk $YBa_2Cu_3O_{7-y}$superconductors, the ideal annealing conditions, and optimum manganese addition amount has triggered thermodynamically the reduction of the stability and the augmentation in the formation of surface nucleation. Correspondingly, the OMn-4 superconductor has been detected to be thermodynamically most unstable [139]. All in all, the E_a values and nucleation stability of materials are known to directly depend on the chemical contents in the composition, couplings between adjacent layers, and interaction between the Mn impurity ions and host ions along the main matrix. Additionally, with the increase in the activation energy value for the crystallization, the penetration of manganese impurity in the bulk $YBa_2Cu_3O_{7-y}$ system has been obtained to be harder as much as possible. Similarly, the shift of crystallization temperatures to higher temperature regions has made the diffusion of manganese impurities to the crystal lattices difficult. Accordingly, both nucleation and crystal growth mechanism have been performed much slower than they should be. Shortly, the impurity ions have been noted to diffuse into the lattice points of bulk OMn-4 superconductor possessing the combination of the highest surface nucleation, and the smallest E_a values and crystallization temperatures. That is to say, the presence of an excess impurity in the $YBa_2Cu_3O_{7-y}$ system has led to a decrease in the nucleation rate for the first crystallization action based on the instantaneous nucleation and 3D parabolic expansion mechanism [135]. The significant reduction of the nucleation rate has retarded the nuclei growth as a consequence of fluctuations of chemical contents in the composition, couplings between adjacent layers, and interaction between the Mn impurity ions and host ions along the main matrix. Consequently, the excess manganese impurity has resulted in damage to the chain reaction process related to the surface nucleation transition into 1D, 2D, and 3D growth [140, 141].

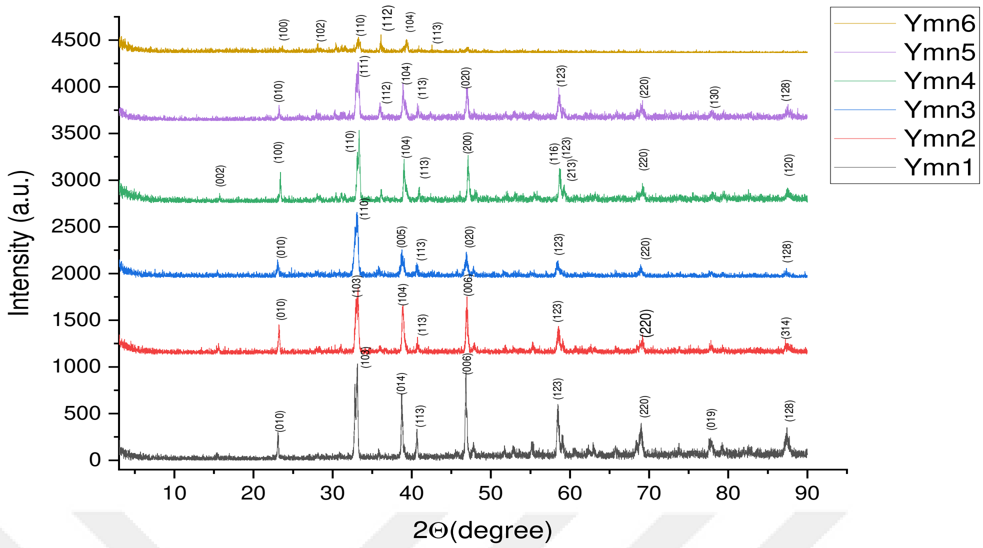

Figure 4.12: Pure and Mn added bulk $YBa_2Cu_3O_{7-y}$ superconductors prepared at without the oxygen ambient condition.

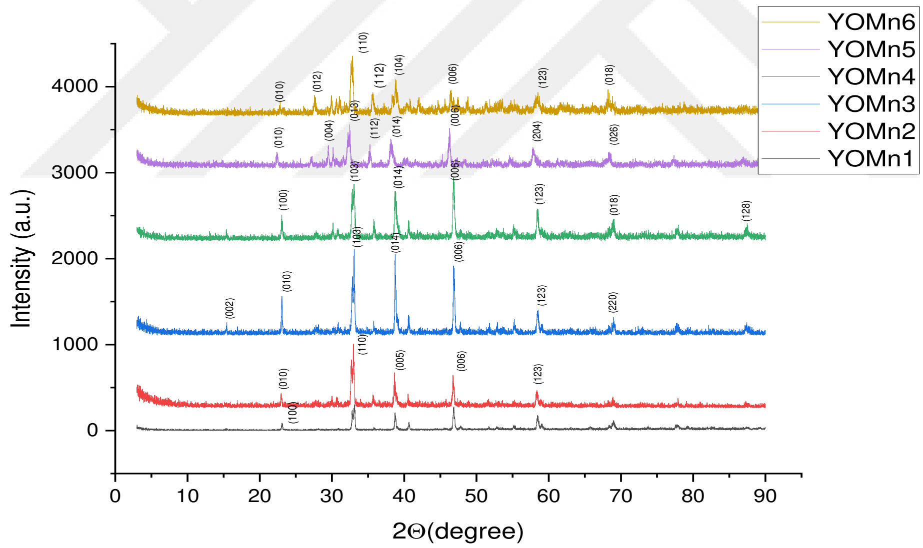

Figure 4.13: Pure and Mn added $YBa_2Cu_3O_{7-y}$ superconductors produced under the oxygen ambient condition.

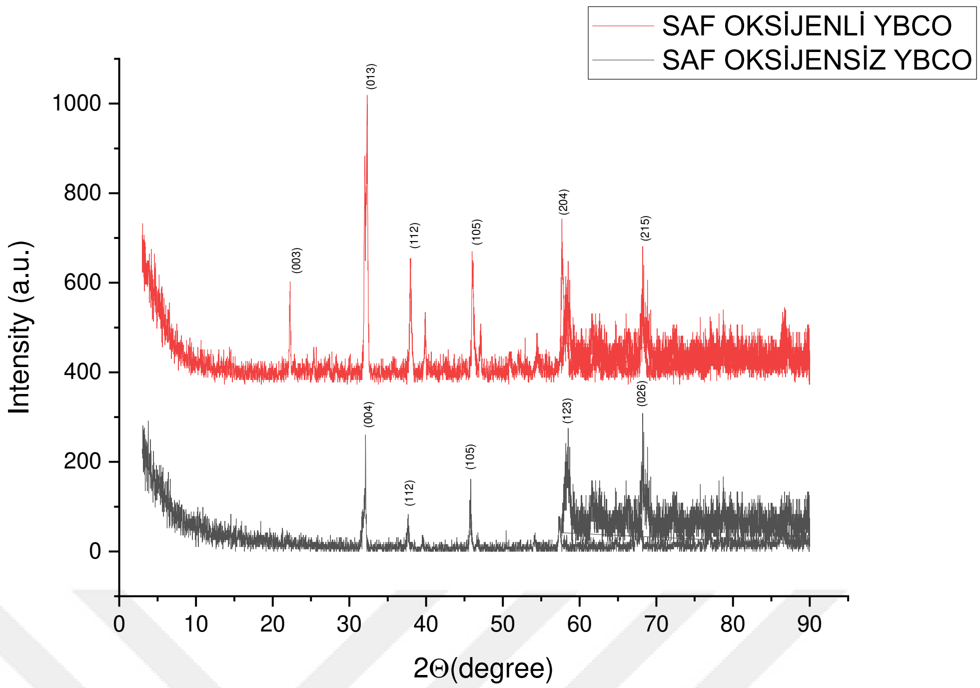

Figure 4.14: YBCO under oxygen and without oxygen.

4.5 EDX Results of Bulk $YBa_2Cu_3O_{7-y}Mn_x$ Systems Prepared

The electron dispersive X-ray (abbreviated as EDX) measurements have experimentally been studied to determine how the chemical components including Y, Mn, Cu, Ba, and O have been distributed (homogeneously and uniformly or not) throughout the bulk $YBa_2Cu_3O_{7-y}Mn_x$ superconductors depending on the oxygen annealing ambient and different manganese impurity addition amount. According to the experimental results obtained from the other parts, it is obvious that the presence of oxygen ambient in the annealing conditions has been observed to affect positively. On this basis, we have provided the distribution of chemical components throughout the bulk $YBa_2Cu_3O_{7-y}Mn_x$ superconductors produced under the oxygen ambient in Table 4.5. It is apparent from the experimental results deduced from Table 4.5 that every chemical composition used has been located in the $YBa_2Cu_3O_{7-y}$ superconductors. Besides, the pure superconductor has been composed of Y, Cu, Ba, and O element compositions. On this basis, all the chemical components have been detected to introduce the main matrix of $YBa_2Cu_3O_{7-y}$ superconductors successfully [30]. This fact has already been verified by the other experimental findings given in the previous sections. Numerically, the signals detected from the K_α and L_α lines have shown that the pure superconductor has contained the molar weights of 13.395 % for the yttrium content, 41.381 % for the barium content, 28.714 % for the copper content, and 16.512 % for the oxygen content. With the increase in the manganese impurity addition amount, the K_α peak related to the manganese content has been realized to appear in the $YBa_2Cu_3O_{7-y}$ main matrix. In fact, the Mn content has been observed to enhance regularly from 0.0702% for the OMn-1 superconductor to 0.812% for the OMn-6 superconductor as the Mn impurity has increased in the crystal system. As for the level of O element composition in the $YBa_2Cu_3O_{7-y}$ superconductor, with increasing the manganese impurity addition level up to x=0.07 in the bulk $YBa_2Cu_3O_{7-y}Mn_x$ superconductors the molar weight has been recorded to augment systematically from 16.512% to 16.775%. Thus, in the case of x=0.07 in the $YBa_2Cu_3O_{7-y}Mn_x$ system, the MnO-4 superconductor has exhibited the molar weight value of 16.775%. Similarly, the same sample has been noted to present the highest copper molar weight value of 28.803%. Correspondingly, it is clear that the molar weights of oxygen and copper contents have determined to be effective role on the basic characteristic features such as electrical, flux pinning ability, superconducting, stabilization of system, morphological, crystallinity quality, pairing mechanism, grain boundary couplings, structural, orbital hybridization mechanisms, andmechanical performance properties. On the other hand, the minimum values for the oxygen and copper molar weights have been observed for the MnO-6 sample. Namely, the copper and oxygen deficits have been found to increase significantly. Moreover, the manganese impurity with the electronegativity, valance electron states, electron configurations, cation-vacancy, ionic radius dimensions, and atomic occupancy ratios has re-organized the $YBa_2Cu_3O_{7-y}$ crystal system due to the variation in the distortion energy and Coulomb interaction in the system. As for the distribution content of barium element, all the $YBa_2Cu_3O_{7-y}$ samples have presented to remain almost constant (with the little deviations stemming from the compensation of manganese gain in the main matrix) at the molar weight of approximately 41% for all the superconductors. Additionally, we have examined the change of molar weight belonging to the Y element content in the $YBa_2Cu_3O_{7-y}$ main matrix. It has been found that the molar weight of yttrium has been recorded to decrease monotonously from 13.395% for the pure sample until the value of 13.008% for the MnO-4 superconductor. However, after the impurity addition value of x=0.07 the Y element content has been noted to re-increase rapidly. The change of the chemical composition distribution in the Y element content has confirmed that the foreign manganese impurity has successfully been introduced in the crystal system.

As a result, determining the behavior of the produced materials under different magnetic fields will increase the application of these materials in the fields of technology, industry and engineering.

Table 4. 5: Distribution of chemical components throughout the bulk $YBa_2Cu_3O_{7-y}Mn_x$ superconductors produced under the oxygen ambient.

Component	Line	Distribution Content (molar wt.%)						
		Pure	OMn-1	OMn-2	OMn-3	OMn-4	OMn-5	OMn-6
Y	K_α	13,395	13,362	13,411	13,385	13,008	13,377	13,349
Ba	L_α	41,381	41,315	41,044	41,21	41,032	41,041	40,378
Cu	K_α	28,714	28,728	28,745	28,774	28,803	28,386	27,783
O	K_α	16,512	16,525	16,586	16,602	16,775	16,396	16,102
Mn	K_α	-------	0,0702	0,214	0,326	0,385	0,812	2,395

5. REFERENCES

“Vancouver citation system was used in this thesis.”

1. Holleman, Arnold F.; Wiberg, Egon; Wiberg, Nils (1985). "Mangan". Lehrbuch der AnorganischenChemie (in German) (91–100 ed.). Walter de Gruyter. pp. 1110–1117. ISBN 978-3-11-007511-3.

2. By William F. Cannon, Bryn E. Kimball, and Lisa A. Corathers,Manganese USGS 2006

3. Dastur, Y. N.; Leslie, W. C. (1981). "Mechanism of work hardening in Hadfield manganese steel". Metallurgical Transactions A. 12 (5): 749–759. Bibcode:1981MTA....12..749D. doi:10.1007/BF02648339. S2CID 136550117.

4. Stansbie, John Henry (2007). Iron and Steel. Read Books. pp. 351–352. ISBN 978-1-4086-2616-0.

5. Brady, George S.; Clauser, Henry R.; Vaccari. John A. (2002). Materials Handbook: an encyclopedia for managers, technical professionals, purchasing and production managers, technicians, and supervisors. New York, NY: McGraw-Hill. pp. 585–587. ISBN 978-0-07-136076-0.

6. Zhang, Wensheng; Cheng, Chu Yong (2007). "Manganese metallurgy review. Part I: Leaching of ores/secondary materials and recovery of electrolytic/chemical manganese dioxide". Hydrometallurgy. 89 (3–4): 137–159. doi:10.1016/j.hydromet.2007.08.010

7. Verhoeven, John D. (2007). Steel metallurgy for the non-metallurgist. Materials Park, Ohio: ASM International. pp. 56–57. ISBN 978-0-87170-858-8.

8. "Chemical properties of 2024 aluminum allow". Metal Suppliers Online, LLC. Retrieved 30 April 2009.

9. Mccray, W. Patrick (1998). "Glassmaking in renaissance Italy: The innovation of venetian cristallo". JOM. 50 (5): 14–19. Bibcode:1998JOM....50e..14M. doi:10.1007/s11837-998-0024-0. S2CID 111314824.

10. Leigh A. Graham; Alison R. Fout; Karl R. Kuehne; Jennifer L. White; BhaskarMookherji; Fred M. Marks; Glenn P. A. Yap; Lev N. Zakharov; Arnold L. Rheingold & Daniel Rabinovich (2005). "Manganese(I) poly(mercaptoimidazolyl)borate complexes: spectroscopic and structural characterization of MnH–B interactions in solution and in the solid state". Dalton Transactions (1): 171–180. doi:10.1039/b412280a. PMID 15605161.

11. Takeda, A. (2003). "Manganese action in brain function". Brain Research Reviews. 41 (1): 79–87. doi:10.1016/S0165-0173(02)00234-5. PMID 12505649. S2CID 1922613.

12. Shepard, Anna Osler (1956). "Manganese and Iron–Manganese Paints". Ceramics for the Archaeologist. Carnegie Institution of Washington. pp. 40–42. ISBN 978-0-87279-620-1.

13. Kuwahara, Raymond T.; Skinner III, Robert B.; Skinner Jr., Robert B. (2001). "Nickel coinage in the United States". Western Journal of Medicine. 175 (2): 112–114. doi:10.1136/ewjm.175.2.112. PMC 1071501. PMID 11483555.

14. "WSK1216" (PDF). vishay. Vishay Intertechnology. Retrieved 30 April 2022.

15. Dell, R. M. (2000). "Batteries fifty years of materials development". Solid State Ionics. 134 (1–2): 139–158. doi:10.1016/S0167-2738(00)00722-0

16. Chen, Daquin; Zhou, Yang; Zhong, Jiasong (2016). "A review on Mn4+ activators in

solids for warm white light-emitting diodes". RSC Advances. 6 (89): 86285–86296. Bibcode:2016RSCAd...686285C. doi:10.1039/C6RA19584A.

17. Jansen, Thomas; Baur, Florian; Jüstel, Thomas (2017). "Red emitting K2NbF7:Mn4+ and K2TaF7:Mn4+ for warm-white LED applications". Journal of Luminescence. 192: 644–652. Bibcode:2017JLum..192..644J. doi:10.1016/j.jlumin.2017.07.061.

18. Zhou, Zhi; Zhou, Nan; Xia, Mao; Yokoyama, Meiso; Hintzen, H. T. (Bert) (6 October 2016). "Research progress and application prospects of transition metal Mn4+-activated luminescent materials". Journal of Materials Chemistry C. 4 (39): 9143–9161. doi:10.1039/c6tc02496c.

19. Y. Zalaoglu, E. Bekiroglu, M. Dogruer, G. Yildirim, O. Ozturk, C. Terzioglu, Comparative study on mechanical properties of undoped and Ce-doped Bi-2212 superconductors, J. Mater. Sci. Mater. El. 24 (7) (2013) 2339–2345.

20. H.K. Onnes, Further experiments with liquid helium. D. On the change of electrical resistance of pure metals at very low temperatures, etc. V. The disappearance of the resistance of mercury, K. Ned. Akad. van Wet. Proc. (in: Koninklijke Nederlandsche Akademie van Wetenschappen Proceedings) 14 (1911) 113–115.

21. R. Kleiner, W. Buckel, Superconductivity an introduction, Wiley-VCH, New York, 3th Ed., (2016).

22. S.B. Guner, Y. Zalaoglu, T. Turgay, O. Ozyurt, A.T. Ulgen, M. Dogruer, G. Yildirim, A detailed research for determination of Bi/Ga partial substitution effect in Bi-2212 superconducting matrix on crucial characteristic features, J. Alloy. Compd. 772 (2019) 388–398.

23. J.G. Bednorz, K.A. Muller, Possible High-T_c Superconductivity in the Ba-La-Cu-O System, Z. Phys. B 64 (1986) 189–193.

24. Saunders, P.J.; Ford, G.A. (2005). The Rise of the Superconductors. Boca Raton, FL: CRC Press.

25. P. Bordet, C. Chaillout, J. Chenavas, J.L. Hodeau, M. Marezio, J. Karpinski, E. Kaldis, Structure Determination of the New High-Temperature Superconductor $Y_2Ba_4Cu_7O_{14+X}$, Nature 336 (1988) 596–599.

26. P. Marsh, R.M. Fleming, M.L. Mandich, A.M. Desantolo, J. Kwo, M. Hong, L.J. Martinez-Miranda, Crystal-Structure of the 80K Superconductor $YBa_2Cu_4O_8$, Nature 334 (1988) 141–143.

27. I.A. Parinov, Microstructure and properties of high-temperature superconductors, Berlin Heidelberg. Springer-Verlag, (2007).

28. V.L. Ginzburg, E.A. Andryushin, Superconductivity, Revised ed. World Scientific Pub. Co. Inc. (2004).

29. M. Pakdil, E. Bekiroglu, M. Oz, N.K. Saritekin, G. Yildirim, Role of preparation conditions of Bi-2223 ceramic materials and optimization of Bi-2223 phase in bulk materials with experimental and statistical approaches, J. Alloy. Compd. 673 (2016) 205–214.

30. A.T. Ulgen, T. Turgay, C. Terzioglu, G. Yildirim, M. Oz, Role of Bi/Tm substitution in Bi-2212 system on crystal structure quality, pair wave function and polaronic states, J. Alloy. Compd. 764 (2018) 755–766.

31. U. Erdem, Y. Zalaoglu, A.T. Ulgen, T. Turgay, G. Yildirim, Role of trivalent Bi /Tm partial substitution on active operable slip systems in Bi 2212 crystal structure, Cryogenics, 113 (2021) 103212.

32. S.Y. Oh, H.R. Kim, Y.H. Jeong, O.B. Hyun, C.J. Kim, Joining of Bi-2212 high-Tc superconductors and metals using indium solders, Physica C 463–465 (2007) 464–467.

33. F.N. Werfel, U. Floegel-Delor, R. Rothfeld, T. Riedel, B. Goebel, D. Wippich, P. Schirrmeister, Superconductor bearings, flywheels and transportation, Supercond. Sci. Technol. 25 (2012) 014007.

34. T.A. Coombs, A finite element model of magnetization of superconducting bulks using a solid-state flux pump, IEEE T. Appl. Supercond. 21 (2011) 3581–3586.

35. M.E. Takayama,High-pressure synthesis of homologous series of high critical temperature (T_c) superconductors, Chem. Mater. 10 (1998) 2686–2698.

36. H. Yamauchi, M. Karppinen,Application of High-Pressure Techniques: Stabilization and Oxidation-State Control of Novel Superconductive and Related Multi-Layered Copper Oxides, Supercond. Sci. Techol. 13 (2000) R33–R52.

37. T.P. Sheahen, Introduction to High-temperature Superconductivity, 1st ed., Kluwer Academic Publishers, New York, Boston, 2002

38. A.K. Saxena, High-Temperature Superconductors, 2^{nd} Ed., Springer Heidelberg New York Dordrecht London, 2012.

39. G. Yildirim, Determination of optimum diffusion annealing temperature for Au surface-layered Bi-2212 ceramics and dependence of transition temperatures on disorders, J. Alloy. Compd. 699 (2017) 247–255.

40. B. Batlogg, Cuprate superconductors: Science beyond high T(c), Solid State Commun. 107 (1998) 639–647.

41. A.T. Ulgen, U. Erdem, Y. Zalaoglu, T. Turgay, G. Yildirim, Effect of vanadium addition on fundamental electrical quantities of Bi-2223 crystal structure and semi-empirical model on structural disorders-defects,J. Mater. Sci: Mater. El., 31 (2020) 13765–13777.

42. M. Runde, Application of high-T_c superconductors in aluminum electrolysis plants, IEEE T. Appl. Supercond. 5 (1995) 813–816.

43. S. Nagaya, N. Hirano, M. Naruse, T. Watanabe, T. Tamada, Development of a high-efficiency conduction cooling technology for SMES coils, IEEE T. Appl. Supercond. 23 (2013) 5602804–5602807.

44. W. Buckel, R. Kleiner, Superconductivity: Fundamentals and Applications, 2^{nd} ed., Wiley-VCH Verlag, Weinheim, (2004).

45. K. Salama, V. Selymanickam, L. Gao, K. Sun, High-current Density in Bulk $YBa_2Cu_3O_x$ superconductor, Appl. Phys. Lett. 54 (1989) 2352–2354.

46. Zalaoglu, Y., Erdem, U., Bolat, F. C., Akkurt, B., Turgay, T., & Yildirim, G. (2021). Improvement in fundamental electronic properties of Bi-2212 electroceramics with trivalent Bi/Tm substitution: a combined experimental and empirical model approach. Journal of Materials Science: Materials in Electronics, 1-13.

47. M.B. Turkoz, M. Oz, T. Turgay, G. Yildirim, Gece Kitapligi, Evaluation of Magneto-Resistivity performances and Flux Pinning Centers with Vanadium Addition in Bi-2223 Main Matrix, pp. 139 -158, Ankara, Turkey

48. H. Hilgenkamp, J. Mannhart, Grain boundaries in high T_c superconductors, J. Rev. Mod. Phys. 74 (2002) 485–549.

49. C. Autret-Lambert, B. Pignon, M. Gervais, I. Monot-Laffez, A. Ruyter, L. Ammor, F. Gervais, J.M. Bassat, R. Decourt, Microstructural and transport properties in substituted $Bi_2Sr_2CaCu_2O_{8+delta}$ modulated compounds, J. Solid State Chem. 179 (2006) 1698–1706.

50. F. Ben Azzouz, M. Zouaoui, K.D. Mani, M. Annabi, G. Van Tendeloo, M. Ben Salem, Structure, microstructure and transport properties of B-doped YBCO system, Phys. C Supercond. Its Appl. 442 (2006) 13–19. doi:10.1016/j.physc.2006.03.135.

51. J.J. Roa, E. Jiménez-Piqué, X.G. Capdevila, M. Segarra, Nanoindentation with spherical tips of single crystals of YBCO textured by the Bridgman technique: Determination of indentation stress-strain curves, J. Eur. Ceram. Soc. 30 (2010) 1477–1482. doi:10.1016/j.jeurceramsoc.2009.10.021.

52. S. Dadras, S. Dehghani, M. Davoudiniya, S. Falahati, Improving superconducting properties of YBCO high temperature superconductor by Graphene Oxide doping, Mater. Chem.Phys. 193 (2017) 496–500. doi:https://doi.org/10.1016/j.matchemphys.2017.03.003.

53. K. Salama, V. Selymanickam, L. Gao, K. Sun, High-current Density in Bulk $YBa_2Cu_3O_x$ superconductor, Appl. Phys. Lett. 54 (1989) 2352–2354.

54. I.A. Parinov, Microstructure and Properties of High-Temperature Superconductors, Springer Berlin Heidelberg, 2007.

55. L. Zhou, P. Zhang, P. Ji, K. Wang, X. Wu, The properties of YBCO Superconductors prepared by a new approach-the powder melting process, Supercond. Sci. Technol. 3 (1990) 490–492.

56. Ajay Kumar Saxena High-Temperature Superconductors Second Edition, Springer-Verlag Berlin Heidelberg 2010,2012

57. M. H. Whangbo, & C. C. Torardi, Hole density dependence of the critical temperature and coupling constant in the cuprate superconductors. Science, 249 (4973) (1990) 1143-1146. https://doi.org/10.1126/science.249.4973.11434

58. M. Kikuchi, M. Y. Syono, Y. A. Tokiwa, K. Oh-ishi, H. Arai, K. Hiraga, N. Kobayashi, T. Sasaoka, Y. Muto, Thermal and X-ray analyses of high temperature superconductor $YBa_2Cu_3O_{6.74}$. Jpn. J. Appl. Phys, 26 (1987) 1066–1069. https://doi.org/10.1143/JJAP.26.L1066

59. C. Chaillout, P. Bordet, J. Chenavas, J. L. Hodeau, M. Marezio, J. Karpinski, E. Kaldis, S. Rusiecki, Solid State Commun., 70 (1989) 275–278.https://doi.org/10.1016/0038-1098(89)90326-8.

60. A. Hamrita, F. B. Azzouz, A. Madani, M. B. Salem, Magnetoresistivity and microstructure of $YBa_2Cu_3O_y$ prepared using planetary ball milling, Phys. C: Supercond. Appl., 472 (1) (2012) 34–38.https://doi.org/10.1016/j.physc.2011.10.003

61. B. Akkurt, U. Erdem, Y. Zalaoglu, A. T. Ulgen, T. Turgay, G. Yildirim, Evaluation of crystallographic and electrical-superconducting features of Bi-2223 advanced ceramics with vanadium addition. J Mater Sci: Mater Electron 32 (2021) 5035–5049. https://doi.org/10.1007/s10854-021-05238-5

62. H. Li, R. C. Bradt, Themicro-hardness indentation load/size effect in rutile and cassiterite single crystals, J.Mater. Sci. 28 (1993) 917–926.

63. J.C. De Vero, G.R.S. Blanca, J.R. Vitug, W.O. Garcia, R.V. Sarmago, Stoichiometric transfer of material in the infrared pulsed laser deposition of yttrium doped Bi-2212 films, Physica C 471 (11–12) (2011) 378–383.

64. G.R.S. Blanca, J.C. De Vero, W.O. Garcia, R.V. Sarmago, Enhanced flux pinning in IR PLD grown Y-doped Bi-2212 films, Physica C 484 (2013) 74–76.

65. Y. Zalaoglu, E. Bekiroglu, M. Dogruer, G. Yildirim, O. Ozturk, C. Terzioglu, Comparative study on mechanical properties of undoped and Ce-doped Bi-2212 superconductors, J. Mater. Sci. Mater. El. 24 (7) (2013) 2339–2345.

66. H. Jin, J. Kotzler, Effect of La-doping on growth and superconductivity ofBi-2212 crystals, Physica C 325 (1999) 153–158.

67. P.M. Sarun, R. Shabna, S. Vinu, A. Biju, U. Syamaprasad, Highly enhanced superconducting properties of Bi-2212 by Y and Pb co-doping, Physica B 404 (8–11) (2009) 1602–1606.

68. Y. Zalaoglu, E. Bekiroglu, M. Dogruer, G. Yildirim, O. Ozturk, C. Terzioglu, Comparative study on mechanical properties of undoped and Ce-doped Bi-2212 superconductors, J. Mater. Sci. Mater. El. 24 (7) (2013) 2339–2345.

69. A. Sotelo, Sh Rasekh, H. Amaveda, P. Bosque, M.A. Torres, M.A. Madre, J.C. Diez, Textured Pb-Doped Bi-2212 Superconductors for Current Limiters, J. Supercond. Nov. Magn. 28 (2015) 447–452.

70. U. Erdem, Y. Zalaoglu, A.T. Ulgen, T. Turgay, G. Yildirim, Role of trivalent Bi /Tm partial substitution on active operable slip systems in Bi 2212 crystal structure, Cryogenics, 113 (2021) 103212.

71. N.K. Saritekin, Y. Zalaoglu, G. Yildirim, M. Dogruer, C. Terzioglu, A. Varilci, O. Gorur, Determination of solid solubility level of Ho nanoparticles in Y-123 superconducting matrix and strong Cu-1 site preference of nanoparticles, J. Alloys Comp. 610 (2014) 361–371.

72. O. Gorur, Y. Ozturk, G. Yildirim, M. Dogruer, C. Terzioglu, Sn diffusion coefficient and activation energy determined by way of XRD measurement and evaluation of micromechanical properties of Sn diffused YBa2Cu3O7-x superconducting ceramics, J. Mater. Sci.: Mater. Electron. 24 (2013) 3063–3072.

73. H. Eskes, G.A. Sawatzky, Tendency towards local spin compensation of holes in the high-T_c copper-compounds, Phys. Rev. Lett. 61 (1988) 1415–1418.

74. M. Dogruer, G. Yildirim, E. Yucel, C. Terzioglu, Role of diffusion-annealing temperature on the microstructural and superconducting properties of Cu-doped MgB_2 superconductors, J. Mater. Sci: Mater. El. 23 (2012) 1965–1970.

75. G. Burns, High-temperature Superconductivity: an Introduction, Academic Press, New York, (1991).

76. Y. Zalaoglu, F. Karaboga, C. Terzioglu, G. Yildirim, Improvement of mechanical performances and characteristics of bulk Bi-2212 materials exposed to Au diffusion and stabilization of durable tetragonal phase by Au, Ceram. Int. 43 (2017) 6836–6844.

77. R.C. Dynes, A.E. White, J.M. Graybeal, J.P. Garno, Breakdown of Eliashberg theory for two-dimensional superconductivity in the presence of disorder, Phys. Rev. Lett. 57 (1986) 2195-2198.

78. J.M. Graybeal, M.A. Beasley, Localization and interaction effects in ultrathin amorphous superconducting films, Phys. Rev. B 29 (1984) 4167–4169.

79. N. K. Saritekin, M. Pakdil, G. Yildirim, M. Oz, T. Turgay, Decrement in Metastability with Zr Nanoparticles Inserted in Bi-2223 Superconducting System and Working Principle of Hybridization Mechanism, J. Mater. Sci. Mater. El. 27 (2016) 956–965.

80. YILDIRIM, G. (2013). Beginning point of metal to insulator transition for Bi 2223 superconducting matrix doped with Eu nanoparticles. Journal of Alloys and Compounds, 578, 526–535.

81. M.B. Turkoz, S. Nezir, C. Terzioglu, A. Varilci, G. Yildirim, Investigation of Lu effect on YBa2Cu3O7-∟ superconducting compounds, J. Mater. Sci: Mater. El. 24 (2013) 896–905.

82. Y. Zalaoglu, G. Yildirim, H. Buyukuslu, N.K. Saritekin, A. Varilci, C. Terzioglu, O. Gorur, Important defeats on pinning of 2D pancake vortices in highly anisotropic Bi-2212 superconducting matrix with homovalent Bi/La substitution, J. Alloy. Compd. 631 (2015) 111–119.

83. A.K. Saxena, High-temperature superconductors, Springer, Berlin, 2010.

84. M.B. Turkoz, S. Nezir, C. Terzioglu, A. Varilci, G. Yildirim, Investigation of Lu effect on YBa2Cu3O7-∟ superconducting compounds, J. Mater. Sci: Mater. El. 24 (2013) 896–905.

85. S. Martin, M. Gurvitch, C.E. Rice, A.F. Hebard, P.L. Gammel, R.M. Fleming, A.T. Fiory, Nonlinear temperature-dependence of the normal-state resistivity in YBa2Cu4O8γ films, Phys. Rev. B 39 (1989) 9611–9613.

86. R. Shabna, P.M. Sarun, S. Vinu, U. Syamaprasad, Charge carrier localization and metal to insulator transition in cerium substituted (Bi,Pb)-2212 superconductor, J. Alloy. Compd. 493 (2010) 11–16.

87. D.M. Newns, P.C. Pattnaik, C.C. Tsuei, Role of vanhove singularity in high-temperature superconductors - Mean field, Phys. Rev. B 43 (1991) 3075–3084.

88. D.M. Newns, P.C. Pattnaik, C.C. Tsuei, Role of van hove singularity in high-temperature superconductors: Mean field, Phys. Rev. B 43 (1991) 3075–3084.

89. S. Martin, M. Gurvitch, C.E. Rice, A.F. Hebard, P.L. Gammel, R.M. Fleming, A.T. Fiory, Nonlinear temperature-dependence of the normal-state resistivity in YBa2Cu4O8γ films. Phys. Rev. B 39 (1989) 9611–9613.

90. R. Shabna, P.M. Sarun, S. Vinu, U. Syamaprasad, Charge carrier localization and metal to insulator transition in cerium substituted (Bi,Pb)-2212 superconductor, J. Alloy. Compd. 493 (2010) 11–16.

91. M.B. Turkoz, S. Nezir, C. Terzioglu, A. Varilci, G. Yildirim, Investigation of Lu effect on YBa2Cu3O7- superconducting compounds, J. Mater. Sci: Mater. El. 24 (2013) 896–905.

92. Y. Zalaoglu, G. Yildirim, H. Buyukuslu, N.K. Saritekin, A. Varilci, C. Terzioglu, O. Gorur, Important defeats on pinning of 2D pancake vortices in highly anisotropic Bi-2212 superconducting matrix with homovalent Bi/La substitution, J. Alloy. Compd. 631 (2015) 111–119.

93. H. Yamauchi, M. Karppinen, Application of High-Pressure Techniques: Stabilization and Oxidation-State Control of Novel Superconductive and Related Multi-Layered Copper Oxides, Supercond. Sci. Techol. 13 (2000) R33–R52.

94. Plakida, N. (2010). High Temperature Cuprate Superconductors. Springer Series in Solid-State Sciences. Springer. p. 480. ISBN 9783642126321.

95. A. Biju, P.M. Sarun, R.P. Aloysius, U. Syamaprasad, Flux pinning properties of Yb substituted (Bi,Pb)-2212 superconductor, J. Alloy. Compd. 454 (2008) 46–51.

96. M.B. Turkoz, M. Oz, T. Turgay, G. Yildirim, Gece Kitapligi, Evaluation of Magneto-Resistivity performances and Flux Pinning Centers with Vanadium Addition in Bi-2223 Main Matrix, pp. 139 -158, Ankara, Turkey

97. E. K. H. Salje, A. S. Alexandrov, W. Y. Liang, Polarons and bipolarons in High-Tc superconductors and related materials, Cambridge University Press, (1995).

98. G. M. Zhao, Experimental constraints on the physics of cuprates, Philosophical Mag. B 81 (2001) 1335.

99. M. Sahoo, D. Behera., Effect of Ti Doping on Structural and Superconducting Property of YBa2Cu3O7−y High Tc Superconductor J Supercond Nov Magn (2014) 27:83–93[Vanadium]

100. R. Awad, A.I. Abou-Aly, M.M.H. Abdel Gawad, I. G-Eldeen, The influence of SnO_2 nano-particles addition on the vickers microhardness of (Bi, Pb)-2223 superconducting phase, J. Supercond. Nov. Magn. 25 (2012) 739–745.

101. E. Silva, S. Sarti, R. Fastampa, M. Giura, Phys. Rev. B 65 (2001) 144508.

102. L.G. Aslamazov, A.I. Larkin, Sov. Phys 10 (1968) 875.

103. Monthoux, P.; Balatsky, A.; Pines, D. (1992). "Weak-coupling theory of high-temperature superconductivity in the antiferromagnetically correlated copper oxides". Physical Review B. 46 (22):1480314817. Bibcode:1992PhRvB..4614803M. doi:10.1103/PhysRevB.46.14803. PMID 10003579

104. W.E. Lawrence, S. Doniach, in: Proc. 12th International Conf. Low Temperature Physics (Keigaku, Tokyo) Eizo Kanada, 1970, p. 361.

105. S.A. Saleh, S.A. Ahmed, E.M.M. Elshikh, J. Supercond. Nov. Magnetism 21 (2008) 187.

106. W.J. Allen, C.G. Olson, MRS Bull. 34, (1990)

107. M.H. Whangbo et al., in *High Temperature Superconducting Materials: Synthesis, Properties and Processing*, ed. by W.E. Halfield, J.H. Miller (Marcel-Dekker, New York, 1988), p. 181

108. M.H. Whangbo et al., Inorg. Chem. 26, 1829 (1987)

109. M.H. Whangbo, C.C. Torardi, Acc. Chem. Res. 24, 133–139 (1991)

110. H. Eskes, G.A. Sawatzky, Tendency towards local spin compensation of holes in the high-T_c copper-compounds, Phys. Rev. Lett. 61 (1988) 1415–1418.

111. G. Burns, High-temperature Superconductivity: an Introduction, Academic Press, New York, (1991).

112. Y. Zalaoglu, F. Karaboga, C. Terzioglu, G. Yildirim, Improvement of mechanical performances and characteristics of bulk Bi-2212 materials exposed to Au diffusion and stabilization of durable tetragonal phase by Au, Ceram. Int. 43 (2017) 6836–6844.

113. R.C. Dynes, A.E. White, J.M. Graybeal, J.P. Garno, Breakdown of Eliashberg theory for two-dimensional superconductivity in the presence of disorder, Phys. Rev. Lett. 57 (1986) 2195-2198.

114. J.M. Graybeal, M.A. Beasley, Localization and interaction effects in ultrathin amorphous superconducting films, Phys. Rev. B 29 (1984) 4167–4169.

115. M.V. Feigelman, V.B. Geshkenbein, A.I. Larkin, V.M. Vinokur, Theory of collective flux creep, Phys. Rev. Lett. 63 (1989) 2303–2306.

116. M.P.A. Fisher, Vortex-Glass superconductivity: A possible new phase in bulk high T_c oxides, Phys. Rev. Lett. 62 (1989) 1415–1418.

117. V.V. Schmidt, P. Muller, A.V. Ustinov, I.V. Grigorieva, The Physics of Superconductors: Introduction to Fundamentals and Applications, 1st ed., Springer, Berlin, 2010.

118. J. Horvat, S. Soltanian, X.L. Wang, S.X. Dou, Effect of sample size on magnetic J_c for MgB_2 superconductor, Appl. Phys. Lett. 84 (2004) 3109–3111.

119. M. Tinkham, Introduction to Superconductivity, 2nd ed., McGraw-Hill, New York, 1996

120. J.B. Ketterson, S.N. Song, Superconductivity, 1st ed., Cambridge University Press, Cambridge, 1999

121. G. Yildirim, M. Dogruer, F. Karaboga, C. Terzioglu, Formation of nucleation centers for vortices in Bi-2223 superconducting core by dispersed Sn nanoparticles, J. Alloy. Compd. 584 (2014) 344–351.

122. D. Dew-Hughes,Flux pinning mechanisms in type-II superconductors, Phil. Mag. 30 (1974) 293–305.

123. E.H. Brandt, The flux-line lattice in superconductors, Rep. Prog. Phys. 58 (1995) 1465–1594

124. S. Gupta, R.S. Yadav, N.P. Lalla, G.D. Verma, B. Das, Microstructural and Superconducting Properties of $YBa_2Cu_{3-x}Co_xO_{7-\delta}$ System, Integr. Ferroelectr. 116 (2010) 68–81.

125. G. Yildirim, M. Dogruer, F. Karaboga, C. Terzioglu, Formation of nucleation centers for vortices in Bi-2223 superconducting core by dispersed Sn nanoparticles, J. Alloy. Compd. 584 (2014) 344–351.

126. D. Dew-Hughes,Flux pinning mechanisms in type-II superconductors, Phil. Mag. 30 (1974) 293–305.

127. E.H. Brandt, The flux-line lattice in superconductors, Rep. Prog. Phys. 58 (1995) 1465–1594.

128. S. Gupta, R.S. Yadav, N.P. Lalla, G.D. Verma, B. Das, Microstructural and Superconducting Properties of $YBa_2Cu_{3-x}Co_xO_{7-\delta}$ System, Integr. Ferroelectr. 116 (2010) 68–81.

129. *Khare, Neeraj (2003).* Handbook of High-Temperature Superconductor Electronics. *CRC Press.* ISBN 978-0-8247-0823-8

130. M. Sahoo, D. Behera Effect of Ti Doping on Structural and Superconducting Property of YBa2Cu3O7−y High Tc Superconductor J Supercond Nov Magn (2014) 27:83–93

131. E. Hannachi, Y. Slimani, F. Ben Azzouz, A. Ekicibil, Higher intra-granular and inter-granular performances of YBCO superconductor with TiO2 nano-sized particles addition, Ceramics International, 44, 15, 18836-18843

132. Kulpa, A., Chaklader, A.C.D., Osborne, N.R., Roemer, G., Sullivan, B., Williams, D.L.: Influence of oxygen ordering and sintering temperatures on the superconducting transition temperature of YBa2Cu3Ox compound at fixed oxygen content x higher than x = 6.8. Solid State Commun. 71, 265–268 (1989)

133. A. Yildiz, K. Kocabas, G.B. Akyuz, J. Supercond. Nov. Magn. 25 (2012) 1459–1467.

134. B.D. Cullity, Elements of X-ray Diffraction, third ed., Addition-Wesley, Reading, 2001.

135. T. Kannan, P. Predeep, Investigation into the superconducting threshold of Bi1.6Pb0.4Sr2Can-1CunO2n+4+delta, n=2, 2.5, 4 perovskites synthesized by glassy precursor route with Thermal and Raman spectroscopic techniques, J. Therm. Anal. Calorim., 114 (2013) 635–641.

136. A. Nilson, W. Gruner, J. Acker, K. Wetzig, Critical aspects on preparation of Bi-2223 glassy precursor by melt process. J. Non-Crystalline Solids, 354 (2008) 839–847.

137. H. Koralay, O. Hicyilmaz, S. Cavdar, O. Ozturk, A.T. Tasci, Experimental and heoretical approaches on thermal and structural properties of Zn doped BSCCO glass ceramics, Materials Science-Poland, 34 (2016) 25–32.

138. M.A. Aksan, M.E. Yakinici, Y. Balci, Thermal analysis study of $Bi_2Sr_2Ca_2Er_xO_{10+d}$ glass ceramic system, J. Therm. Anal. Calorim., 81 (2005) 417–423.

139. A. Ianculescu, M. Gartner, B. Despax, V. Bley, Th Lebey, R. Gavrila, M. Modreanu, Optical characterization and microstructure of $BaTiO_{(3)}$ thin films obtained by RF-magnetron sputtering, Appl. Surf. Sci. 253 (2006) 344–348.

140. M.A. Aksan, M.E. Yakinci, Thermal and superconducting properties of glass-ceramic HTc BiSrCa(CuPr)O system, J. Materials Processing Tech. 196 (2008) 365–372

141. A. Karamanov, M. Pelino, Influence of the nucleation time-lag on the activation energy in non-isothermal crystallization, Journal of Non-Crystalline Solids 290 (2001) 173–179.